JHEP

Published for SISSA by Springer

Received: March 25, 2015
Accepted: September 8, 2015
Published: October 7, 2015

Charged slepton flavor post the 8 TeV LHC: a simplified model analysis of low-energy constraints and LHC SUSY searches

Lorenzo Calibbi,[a] **Iftah Galon,**[b] **Antonio Masiero,**[c] **Paride Paradisi**[c] **and Yael Shadmi**[d]

[a] *Service de Physique Théorique, Université Libre de Bruxelles, 1050 Brussels, Belgium*

[b] *Department of Physics and Astronomy, University of California, Irvine, CA 92697, U.S.A.*

[c] *Dipartimento di Fisica ed Astronomia "G.Galilei", Università degli Studi di Padova, and Istituto Nazionale di Fisica Nucleare, Sezione di Padova, Via Marzolo 8, 35131 Padova, Italy*

[d] *Physics Department, Technion-Israel Institute of Technology, Haifa 32000, Israel*

E-mail: calibbi@itp.ac.cn, iftah.galon@gmail.com, antonio.masiero@pd.infn.it, paride.paradisi@pd.infn.it, yshadmi@physics.technion.ac.il

Abstract: Motivated by the null results of LHC searches, which together with the Higgs mass, severely constrain minimal supersymmetric extensions of the standard model, we adopt a model-independent approach to study charged slepton flavor. We examine a number of simplified models, with different subsets of sleptons, electroweak gauginos, and Higgsinos, and derive the allowed slepton flavor dependence in the region probed by current LHC searches, and in the region relevant for the 14 TeV LHC. We then study the impact of the allowed flavor dependence on lepton plus missing energy searches. In some cases, flavor dependence significantly modifies the reach of the searches. These effects may be even larger at the next LHC run, since for the higher masses probed at 14 TeV, larger flavor mixings and relative mass splittings are compatible with low-energy constraints. Retaining the full lepton flavor information can increase the sensitivity of the searches.

Keywords: Supersymmetry Phenomenology

ArXiv ePrint: 1502.07753

doi:10.1007/JHEP10(2015)043

JHEP10(2015)043

Contents

1 Introduction **2**

2 General setup: slepton flavor parameters **4**

3 Leptonic dipoles and low energy observables **5**

4 Simplified models: LFV versus LHC bounds **7**
- 4.1 $\widetilde{\ell}_L\widetilde{B}$ models 8
- 4.2 $\widetilde{\ell}_L\widetilde{W}$ models 10
- 4.3 $\widetilde{\ell}_L\widetilde{B}\widetilde{W}$ models 11
- 4.4 $\widetilde{\ell}_R\widetilde{B}$ models 13
- 4.5 $\widetilde{\ell}_L\widetilde{\ell}_R\widetilde{B}$ models 14
- 4.6 $\widetilde{\ell}_L\widetilde{\ell}_R\widetilde{W}$ models 16
- 4.7 $\widetilde{\ell}_L\widetilde{B}\widetilde{H}$ models 17
- 4.8 $\widetilde{\ell}_R\widetilde{B}\widetilde{H}$ models 19
- 4.9 $\widetilde{\ell}_L\widetilde{W}\widetilde{H}$ models 19
- 4.10 $\widetilde{\ell}_R\widetilde{W}$ models 21
- 4.11 Models with no light gauginos: $\widetilde{\ell}_L\widetilde{H}$, $\widetilde{\ell}_R\widetilde{H}$, $\widetilde{\ell}_L\widetilde{\ell}_R\widetilde{H}$ 21
- 4.12 Heavy superpartner decoupling 22

5 Implications of LFV for LHC searches **22**
- 5.1 $\widetilde{\ell}_L\widetilde{B}$, $\ell = e, \mu$ models 23
- 5.2 $\widetilde{\ell}_R\widetilde{B}$, $\ell = e, \mu$ models 26
- 5.3 $\widetilde{\ell}_L\widetilde{B}$, $\ell = \mu, \tau$ models 28
- 5.4 $\widetilde{\ell}_L\widetilde{B}\widetilde{W}$ models 28
  - 5.4.1 Limits from $\widetilde{\chi}^+\widetilde{\chi}^-$ production 28
  - 5.4.2 Limits from $\widetilde{\chi}^\pm\widetilde{\chi}^0_2$ production 28

6 Conclusions **31**

A Expressions for the leptonic dipoles **33**
- A.1 $\ell_i \to \ell_j\gamma$ 33
- A.2 $(g-2)_\mu$ 35
- A.3 Electron EDM 36
- A.4 Loop functions 36

JHEP10(2015)043

1 Introduction

With the conclusion of the 8 TeV LHC run, supersymmetric extensions of the Standard Model are greatly constrained by a variety of direct searches. In the Minimal Supersymmetric Standard Model (MSSM), squark masses are further constrained by the 125 GeV Higgs mass, which requires either a large stop mixing or heavy stops. In concrete models, the latter typically translate into lower bounds on the remaining squark masses. Thus, it is quite clear that the simplest scenarios, with all superpartners near the TeV scale or below, are ruled out. In particular, the direct production of sleptons, electroweak gauginos and Higgsinos may be the dominant signature of supersymmetry at the LHC. More generally, it is conceivable that only some subset of superpartners may be within reach, motivating a model-independent approach to supersymmetry searches.

In this paper, we therefore adopt a simplified-model approach to study charged slepton flavor. There are several reasons why slepton flavor is interesting. The origin of fermion masses is one of the most puzzling features of the SM, hinting at some underlying flavor theory. TeV-scale sleptons, if they exist, would provide a new portal into the origin of flavor, both indirectly through Charged Lepton Flavor Violation (CLFV), and through LHC measurements of their masses and couplings. Even more importantly at this stage, LHC slepton searches are in general sensitive to slepton flavor. Thus for example, many slepton searches require Opposite Sign Same Flavor (OSSF) electron and muon pairs, assuming degenerate pure flavor states. However, the slepton sector might feature a more generic flavor dependence, i.e. non-degenerate masses of different flavors and/or mixing among flavor states.

The two main questions we will address are therefore:

1. What is the allowed slepton flavor dependence in the regions probed by current and future LHC searches?

2. How are these searches affected if such flavor dependence is indeed present?

Apart from the fact that we want to examine the first question with as few theory assumptions as possible, there are two other reasons for revisiting it now. The first is very simple. As the LHC pushes the superpartner scale to higher values, the allowed flavor mixings, and relative mass splittings in the slepton spectrum can be larger, with potentially important effects for LHC searches. The second is again related to the measured Higgs mass. As is well known, in the MSSM the strongest bounds on CLFV come from dipole transitions. These are enhanced in the presence of large Higgsino-gaugino mixing, and/or left-right slepton mixing, since then the required chirality flip is supplied by the Yukawa vertex or by the slepton propagator. The measured Higgs mass therefore constitutes an important input for CLFV. In some models, the 125 GeV Higgs mass favors a large μ and heavy Higgsinos. If Higgsino diagrams decouple because of a large μ, the CLFV transitions have reduced contributions and large slepton flavor dependence is possible. In the following, we will therefore examine both scenarios with active Higgsinos and scenarios with decoupled Higgsinos. Finally, the use of simplified models will allow for a direct comparison with existing ATLAS and CMS analyses.

JHEP10(2015)043

Indeed, current ATLAS and CMS electroweak searches [1–6] already probe slepton masses up to a few hundred GeV in some cases. Very roughly, searches based on two leptons (electrons and muons) and missing energy, extend to about 500 GeV chargino masses for a zero LSP mass, if charginos decay to substantially lighter left-handed sleptons [4]. Searches based on three leptons are even more sensitive, as they can exclude neutralino/chargino masses up to 700 GeV for an LSP mass below about 350 GeV [6]. Sleptons can also be directly produced via Drell-Yan processes with Z^0/γ^* s-channel exchange, resulting in an opposite sign lepton-pair and missing energy. Because the relevant couplings are relatively small, these lead to the weakest bounds on the slepton and LSP masses. There is no bound for an LSP above $\approx 150 \div 200$ GeV, and for a light LSP the bounds go up to a left-handed (right-handed) slepton mass of 300 GeV (250 GeV) [4]. However, these bounds are very robust, as they only require the presence of a single slepton and the LSP.

We will consider several simplified models, including models used by ATLAS and CMS to interpret the searches for slepton electroweak production. Each of the models contains only a subset of the sleptons, gauginos and Higgsinos. Schematically, the quantity constrained by CLFV bounds is the product of the slepton relative mass splitting and the slepton mixing. Since we are ultimately also interested in scenarios with large mass splittings, we calculate the CLFV observables in terms of the slepton physical masses and mixings. We then use these in section 4 to derive the allowed regions in the slepton flavor parameters for each of the models in the limit of small slepton mass splitting, showing at the same time the limits set by direct LHC searches.

For each model, we also compute the predictions for the muon anomalous Magnetic Dipole Moment (MDM). If the muon $g-2$ measurement [7–10] is interpreted as a deviation from the SM, it requires, in the context of supersymmetry, light sleptons, gauginos and Higgsinos, with substantial $\tan\beta$ enhancement.[1] We note however that in the simple scenarios we discuss, the muon $g-2$ is related to the electron dipole moment by "naive scaling" with the fermion mass,[2] and large values of $g-2$ require a solution of the supersymmetric CP problem.

We then proceed to analyze the possible implications of lepton flavor violation for LHC lepton plus missing energy searches, in models with sleptons, Binos and Winos. We consider DY slepton pair production, chargino pair production and chargino-neutralino pair production. For each, we derive the excluded region for models with non-degenerate sleptons, and for models with some flavor mixing, and compare these to the flavor-blind results.

While we restrict ourselves to a model-independent approach, it is important to stress that slepton flavor violation of the types we consider can arise in concrete and predictive models [14–22]. Indeed, any mechanism which explains fermion masses is likely to control also sfermion masses. This has been utilized in different frameworks to obtain flavor-dependent spectra consistent with CLFV bounds. In particular, scenarios with large mass splittings can be compatible with CLFV constraints in alignment models [23], in which some mechanism, such as flavor symmetries, suppresses flavor mixing [14, 18, 24–26].

[1] As is well known, this discrepancy may be the result of hadronic SM contributions. For a recent review of experimental prospects for settling this question see e.g. [11].

[2] See e.g. [12, 13] for a discussion of how this scaling can be violated by flavor effects.

JHEP10(2015)043

This paper is organized as follows. In section 2, we set the notation for the slepton flavor parameters. In section 3 we introduce the low-energy observables related to leptonic dipoles, and review the current experimental sensitivities as well as future prospects. In section 4, we analyze the low-energy flavor constraints for each of the models. For reference, we show these constraints together with the limits on flavor-blind sleptons from direct LHC searches. We then turn to the signatures of flavor-dependent models at the LHC, and reinterpret several analyses in terms of flavor dependent slepton spectra in section 5. We conclude with some remarks in section 6. Finally, the supersymmetric expressions for the dipole amplitudes are collected in the appendix.

2 General setup: slepton flavor parameters

We begin by explaining our conventions and assumptions. In each of the models we consider, we assume a single dominant source of flavor violation, so that the main signatures of interest can be described using two slepton states. We use L (R) to denote "left-handed" ("right-handed") sleptons. We will mostly assume small LR mixing, so that the two sleptons are predominantly L or R.

Working in the fermion mass basis, with diagonal gaugino-slepton-lepton couplings, we then write the slepton mass matrices as

$$M^2_{LL} = \begin{pmatrix} m^2_{L_1} & \Delta^{12}_{LL} \\ \Delta^{21}_{LL} & m^2_{L_2} \end{pmatrix}, \qquad M^2_{RR} = \begin{pmatrix} m^2_{R_1} & \Delta^{12}_{RR} \\ \Delta^{21}_{RR} & m^2_{R_2} \end{pmatrix}, \tag{2.1}$$

which can be diagonalized through unitary matrices U_L and U_R, respectively, defined as

$$U_L^\dagger M^2_{LL} U_L = \mathrm{diag}(m^2_{\widetilde{\ell}_1}, m^2_{\widetilde{\ell}_2}), \qquad U_R^\dagger M^2_{RR} U_R = \mathrm{diag}(m^2_{\widetilde{e}_1}, m^2_{\widetilde{e}_2}), \tag{2.2}$$

where U_L and U_R read

$$U_L = \begin{pmatrix} \cos\theta_L & -\sin\theta_L \\ \sin\theta_L & \cos\theta_L \end{pmatrix}, \quad U_R = \begin{pmatrix} \cos\theta_R & -\sin\theta_R \\ \sin\theta_R & \cos\theta_R \end{pmatrix}, \tag{2.3}$$

where, for simplicity, we have assumed CP conservation, i.e. $\Delta^{12}_{LL} = \Delta^{21}_{LL}$ and $\Delta^{12}_{RR} = \Delta^{21}_{RR}$. EDMs in these scenarios thus only arise from "flavor-diagonal" phases.[3] The flavor mixing angles $\sin\theta_{L,R}$, $\cos\theta_{L,R}$ are defined as

$$\sin\theta_L \cos\theta_L = \frac{\Delta^{21}_{LL}}{(m^2_{\widetilde{\ell}_1} - m^2_{\widetilde{\ell}_2})}, \qquad \sin\theta_R \cos\theta_R = \frac{\Delta^{21}_{RR}}{(m^2_{\widetilde{e}_1} - m^2_{\widetilde{e}_2})}, \tag{2.4}$$

where $\widetilde{\ell}_1$ and $\widetilde{e}_1$ are the heaviest mass eigenstates.

We will often use the average slepton mass-squared, m^2_M, and the mass splitting Δm_M, given by,

$$m^2_L \equiv (m^2_{\widetilde{\ell}_1} + m^2_{\widetilde{\ell}_2})/2, \qquad \Delta m_L = m_{\widetilde{\ell}_1} - m_{\widetilde{\ell}_2}, \tag{2.5}$$

$$m^2_R \equiv (m^2_{\widetilde{e}_1} + m^2_{\widetilde{e}_2})/2, \qquad \Delta m_R = m_{\widetilde{e}_1} - m_{\widetilde{e}_2}. \tag{2.6}$$

[3] The contribution to EDMs from flavor-changing parameters has been discussed in [12, 27, 28].

JHEP10(2015)043

It is then useful to define the dimensionless MIs as

$$\delta^{21}_{LL} \equiv \frac{\Delta^{21}_{LL}}{m^2_L}\,, \qquad \delta^{21}_{RR} \equiv \frac{\Delta^{21}_{RR}}{m^2_R}\,. \tag{2.7}$$

In the limit of small mass splitting,

$$\delta^{21}_{LL} \approx \frac{\Delta m_L}{m_L}\sin 2\theta_L\,, \qquad \delta^{21}_{RR} \approx \frac{\Delta m_R}{m_R}\sin 2\theta_R\,. \tag{2.8}$$

As we will discuss in detail in the following sections, while LHC searches are sensitive to the slepton masses and mixings separately, CLFV processes essentially constrain the product of the mixing and relative mass splitting, i.e. δ_{LL} and δ_{RR}. These can be small either because the mass splittings are small, or because the mixing is small, as in alignment models [23]. As shown in [29, 30] the MIA gives a good estimate of CLFV constraints even in this latter case. However, for detailed studies of LHC processes with large mass splittings and small mixings we will employ the full expressions for the dipole amplitudes.

For simplicity, we suppress the L, R indices on Δm and θ, whenever only a single mass splitting and a single mixing angle are present.

In some of the models, we also consider left-right slepton mixing. Generically, this mixing is given by a 3×3 matrix, of the form $y_\ell(A - \mu \tan\beta)$, where y_ℓ is the lepton Yukawa matrix. We will neglect the A-terms in the flavor-diagonal left-right mixings, assuming that the main contribution is due to the $\mu \tan\beta$ term, so that the mixing is proportional to the relevant lepton mass. We will consider, however, A-term-induced flavor violation encoded in

$$\delta^{21}_{LR} \equiv \frac{m_{\ell_2} A_{21}}{\sqrt{m^2_L m^2_R}}\,, \qquad \delta^{21}_{RL} \equiv \frac{m_{\ell_1} A_{12}}{\sqrt{m^2_L m^2_R}}\,. \tag{2.9}$$

3 Leptonic dipoles and low energy observables

The search for flavor violation in charged leptons is certainly one of the most interesting goal of flavor physics in the near future. Indeed, neutrino oscillations have shown that lepton flavor is not conserved, and TeV-scale New Physics (NP) can lead to observable CLFV. Among the most interesting CLFV channels are $\mu \to e\gamma$, $\mu \to eee$, $\mu \to e$ conversion in Nuclei as well as τ LFV processes. The current status and future experimental sensitivities for LFV processes as well as the electron EDM are collected in table 1.

In supersymmetric extensions of the SM, new sources of CLFV stem from the soft SUSY-breaking sector since the lepton and slepton mass matrices are generally misaligned [43, 44]. The dominant CLFV effects are captured by the dipole operators,

$$\mathcal{L} = e\frac{m_{\ell_i}}{2}\bar{\ell}_i \sigma_{\mu\nu} F^{\mu\nu}\left(A^{ij}_L P_L + A^{ij}_R P_R\right)\ell_j \qquad i,j = e,\mu,\tau\,, \tag{3.1}$$

which arise from sneutrino-chargino and slepton-neutralino loops. The Lagrangian (3.1) leads to,

$$\frac{\mathrm{BR}(\ell_i \to \ell_j \gamma)}{\mathrm{BR}(\ell_i \to \ell_j \nu_i \bar{\nu}_j)} = \frac{48\pi^3 \alpha_{\mathrm{em}}}{G^2_F}\left(|A^{ij}_L|^2 + |A^{ij}_R|^2\right)\,, \tag{3.2}$$

LFV Process	Present Bound	Future Sensitivity
$\mu^+ \to e^+\gamma$	5.7×10^{-13} [31]	$\approx 6 \times 10^{-14}$ [32]
$\mu^+ \to e^+e^+e^-$	1.0×10^{-12} [33]	$\mathcal{O}(10^{-16})$ [34]
μ^- Au $\to e^-$ Au	7.0×10^{-13} [35]	?
μ^- Ti $\to e^-$ Ti	4.3×10^{-12} [36]	?
μ^- Al $\to e^-$ Al	–	$\mathcal{O}(10^{-16})$ [37, 38]
$\tau^\pm \to \mu^\pm\gamma$	4.4×10^{-8} [39]	$10^{-8} \div 10^{-9}$ [40]
$\tau^\pm \to \mu^\pm\mu^+\mu^-$	2.1×10^{-8} [41]	$10^{-9} \div 10^{-10}$ [40]
Electron EDM	Present Bound	Future Sensitivity
d_e(e cm)	8.7×10^{-29} [42]	?

Table 1. Current experimental bounds and future sensitivities for some low-energy LFV observables and the electron EDM.

and the following model-independent relations hold:

$$\frac{\mathrm{BR}(\ell_i \to \ell_j\ell_k\bar{\ell}_k)}{\mathrm{BR}(\ell_i \to \ell_j\bar{\nu}_j\nu_i)} \simeq \frac{\alpha_{\rm em}}{3\pi}\left(\log\frac{m^2_{\ell_i}}{m^2_{\ell_k}} - 3\right)\frac{\mathrm{BR}(\ell_i \to \ell_j\gamma)}{\mathrm{BR}(\ell_i \to \ell_j\bar{\nu}_j\nu_i)}\,,$$
$$\mathrm{CR}(\mu \to e \text{ in N}) \simeq \alpha_{\rm em} \times \mathrm{BR}(\mu \to e\gamma)\,. \tag{3.3}$$

As a result, the current MEG bound $\mathrm{BR}(\mu \to e\gamma) \sim 5 \times 10^{-13}$ already implies that $\mathrm{BR}(\mu \to eee) \leq 3 \times 10^{-15}$ and $\mathrm{CR}(\mu \to e \text{ in N}) \leq 3 \times 10^{-15}$.

The CLFV transitions are tightly related to the magnetic and electric leptonic dipole moments, which are given by the effective Lagrangian of eq. (3.1) with $\ell_i = \ell_j$. Denoting the anomalous magnetic moments by Δa_ℓ, and the leptonic EDMs by d_ℓ, we can write them as

$$\Delta a_{\ell_i} = m^2_{\ell_i}\,\mathrm{Re}\left(A^{ii}_L + A^{ii}_R\right)\,, \qquad \frac{d_{\ell_i}}{e} = \frac{m_{\ell_i}}{2}\,\mathrm{Im}\left(A^{ii}_L - A^{ii}_R\right)\,. \tag{3.4}$$

Both Δa_{ℓ_i} and d_{ℓ_i} are extremely sensitive probes of new physics. In particular, the current anomaly $a_\mu = (g-2)_\mu/2$ which exhibits a $\sim 3.5\sigma$ discrepancy between the SM prediction and the experimental value [8] $\Delta a_\mu = a_\mu^{\rm EXP} - a_\mu^{\rm SM} = 2.90\,(90) \times 10^{-9}$, reinforces the expectation of detecting $\mu \to e\gamma$, hopefully within the MEG resolutions. In concrete NP scenarios, Δa_ℓ, d_ℓ and $\mathrm{BR}(\ell \to \ell'\gamma)$ are expected to be correlated. However, their correlations crucially depend on the unknown flavor and CP structure of the NP couplings.

We now review the main features of the superpartner contributions to the Lagrangian (3.1). The chiral symmetry breaking source required by the dipole transition can be implemented in three different ways: (i) through a chirality flip on the external fermion line, (ii) through mixing effects in the chargino/neutralino mass matrices, or (iii) through LR or RL mixings in the charged-slepton mass matrix. In (i), the amplitudes are independent of $\tan\beta$, while in (ii) the leading effects are proportional to $\tan\beta$ because of the lepton Yukawa coupling at the Higgsino-lepton-slepton vertex. In (iii), the amplitudes are proportional to the LR/RL mixing $\sim A - \mu\tan\beta$ and therefore grow with $\mu\tan\beta$.

JHEP10(2015)043

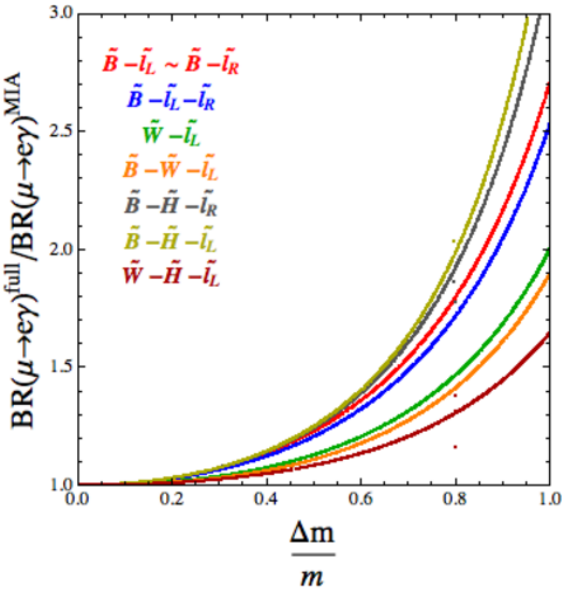

Figure 1. The full vs. MIA results for $\mathrm{BR}(\mu \to e\gamma)$ in the simplified models considered in this paper as a function of the normalized mass-splitting $\Delta m/m$.

In the next section we present the bounds on δ_{MN} in the limit of degenerate slepton masses (for earlier works, see [45–50]). For this purpose, a computation in the so-called Mass Insertion Approximation (MIA) would be sufficient. However, since we are interested also in scenarios with large mass splittings (and small mixings), a full computation in the mass-eigenstate basis is unavoidable. In the appendix we provide very compact expressions for the $\ell_i \to \ell_j\gamma$ amplitudes, distinguishing among the ways in which the chirality flip is implemented. We also collect the expressions for the muon $g-2$, and the electron EDM. In order to simplify the expressions as much as possible while keeping all the important features, these are obtained by treating SU(2) breaking effects in the chargino/neutralino mass-matrices as perturbations [48], and working within a two family framework.

For completeness, we also show in the appendix the MIA amplitudes for $\ell_i \to \ell_j\gamma$. In order to appreciate the limit of validity of the MIA results compared to the full results in the mass-eigenstates, we plot in figure 1 the ratio $\mathrm{BR}(\mu \to e\gamma)^{\mathrm{full}}/\mathrm{BR}(\mu \to e\gamma)^{\mathrm{MIA}}$ for the different simplified models we will discuss in the following, as a function of the normalized mass-splitting $\Delta m/m$ where m is the average slepton mass. As we can see, the two calculations are completely equivalent in the limit $\Delta m/m \to 0$. Moreover, the MIA results are still reasonably accurate up to mass splitting of order $\Delta m/m \lesssim 0.5$, while they underestimate the result for larger mass splittings.

4 Simplified models: LFV versus LHC bounds

In this section, we analyze the implications of the current CLFV bounds for different simplified models, and display the excluded regions together with the results of LHC searches for sleptons and charginos/neutralinos. The latter assume flavor-blind sleptons, with de-

JHEP10(2015)043

generate selectrons and smuons, and no flavor mixing.[4] In this section, we simply display the limits from CLFV experiments together with the LHC limits. In the next section, we discuss the possible effects of relaxing the assumption of flavor blind sleptons, and address the impact of large inter-generation mixing, or mass splittings, on LHC searches.

For simplicity, we restrict ourselves to models defined by at most three mass scales. We denote each model by the light superpartners it contains. For example, in $\widetilde{\ell}_R\widetilde{B}$ models, the only superpartners are right-handed sleptons and a Bino-like lightest neutralino. All other sleptons, neutralinos and charginos are assumed to be very heavy, so that they are beyond the reach of the LHC, and furthermore, their contributions to the various dipole transitions can be neglected. The latter is a much stronger assumption. Indeed, the cross sections for producing heavy superpartner pairs fall very fast with the superpartner mass, whereas the contributions of heavy superpartners to CLFV processes decouple more slowly. We will address this point in detail at the end of this section, and show the parameter ranges for which the simplified expressions of each model represent a good approximation of the full amplitude of the CLFV processes.

We focus here on LHC searches for leptons plus missing energy, which require a neutralino LSP [1–6]. Different hierarchies are possible of course, with the charged slepton NLSP decaying to a gravitino or through R-parity violating couplings. The LHC signatures then depend on the NLSP lifetime and decay products. Thus for example, a single long-lived, left-handed slepton is excluded for masses below 339 GeV based only on its Drell-Yan production [52]. From this, the direct production bound on two (three) degenerate slepton flavors can be estimated to be 400 (435) GeV [26]. Flavor effects in such scenarios were studied for example in [14, 53, 54].

4.1 $\widetilde{\ell}_L\widetilde{B}$ models

We begin with one of the simplest models, with only the left-handed sleptons and a Bino neutralino. This model is a good starting point for understanding some of the main features of the flavor-collider interplay. On the one hand, the left-handed sleptons have larger Drell-Yan production cross-sections compared to the right-handed sleptons. Consequently, LHC searches have a higher reach for left-handed slepton masses. On the other hand, the couplings of left-handed sleptons to the Bino are a factor of 2 smaller than the couplings of right-handed sleptons. The left-handed slepton masses are therefore less constrained by flavor measurements.

The various dipole amplitudes are very simple in this case. Using the expressions collected in the appendices,

$$\begin{aligned} A_L &= (A_L^{n_1})_{U(1)}\,, & A_R &\simeq 0\,. \\ \Delta a_\mu &= \left(\Delta a_\mu^{n_1}\right)^L_{U(1)}\,, & d_e &\simeq 0\,. \end{aligned} \tag{4.1}$$

Thus for example, for small slepton mass splitting, the amplitude for $\mu \to e\gamma$ reads

$$A_L = \frac{\alpha_Y}{4\pi}\frac{\delta^{21}_{LL}}{m_L^2} f_{1n}(x_{1L})\,. \tag{4.2}$$

[4] A notable exception is [51], where separate limits on the selectron and smuon masses are shown in the auxiliary plots.

JHEP10(2015)043

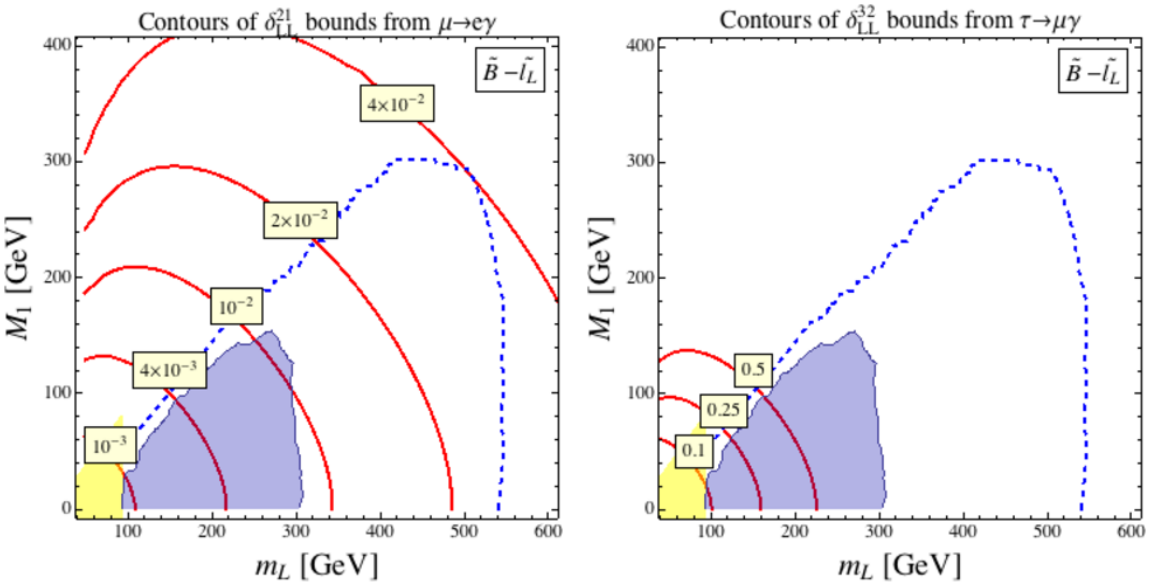

Figure 2. Upper limits on δ_{LL}^{21} (left) and δ_{LL}^{32} (right) in the plane of the Bino mass, M_1, and common L-slepton mass, m_L for the model $\widetilde{\ell}_L B$. The light-blue area is excluded by the ATLAS [1] direct search (assuming flavor blind sleptons), the yellow region refers to the LEP exclusion. The dashed line refers to the future LHC limit with $\sqrt{s} = 14\,\text{TeV}$ and $\mathcal{L} = 100\ \text{fb}^{-1}$, as estimated in [55].

A few features of this model are worth stressing. First, the electron EDM, d_e, vanishes. The required chirality flip can only occur on an external fermion line. The two Bino-lepton-slepton loop-vertices are therefore complex-conjugates of each other. Consequently, the loop amplitude is real and the EDM vanishes. Second, as Δa_μ is always negative, the muon $g-2$ anomaly cannot be accounted for in this scenario. Furthermore, the contribution is numerically small, so that the model predicts a SM-like muon $g-2$.

Third, and most importantly for our purposes, it is straightforward to compare the reach of direct LHC lepton plus missing energy searches [1–6] to $\ell_i \to \ell_j\gamma$ constraints in this case. Since we assume that the Higgsinos are decoupled, and that the only light sleptons are purely left-handed, the relevant LHC signatures as well as the LFV constraints are determined solely by the Bino mass M_1, and, in the limit of flavor blind slepton masses, the slepton mass m_L.

In figure 2, we show the region excluded by the ATLAS search [1],[5] which assumes flavor blind sleptons, together with the constraints from $\mu \to e\gamma$ (left panel) or $\tau \to \mu\gamma$ (right panel) in the $(m_L,\ M_1)$ plane. As noted above, in the absence of flavor dependence, these are the physical masses of the Bino and sleptons in this model. The contours correspond to the upper bounds on $\delta_{LL}^{21} \equiv \Delta_{LL}^{21}/m_L^2$ (left) and $\delta_{LL}^{32} \equiv \Delta_{LL}^{32}/m_L^2$ (right), obtained using the latest limits on $\text{BR}(\ell_i \to \ell_j\gamma)$ listed in table 1. The yellow region represents the LEP exclusion. The light-blue area is excluded by the ATLAS search for Drell-Yan

[5]We choose to show the results of the ATLAS preliminary analysis [1] instead of those of the published paper [4] for the sake of consistency with the numerical results, cf. the next section. We notice however that in terms of limits on the slepton-neutralino mass plane, the two analyses are practically equivalent.

JHEP10(2015)043

slepton pair production, with each slepton decaying to a Bino plus lepton, leading to two Opposite Sign, Same Flavor (OSSF) leptons (e^+e^- and $\mu^+\mu^-$) plus missing transverse momentum [1]. Note that this is the only possible channel for slepton production in these models for $m_L > M_1$. For m_L above or near M_1, the LHC signatures of the model are qualitatively different, and depend in particular on the identity and mass of the LSP, which determine the slepton lifetime. Thus for example, three mass-degenerate long-lived left-handed sleptons are excluded up to 430 GeV [26, 52].

We see that in the light-blue region probed by the LHC, the allowed flavor dependence can be substantial. There are essentially no constraints on the stau-smuon system, and even in the selectron-smuon system, δ^{21}_{LL} at the percent level is allowed. We also show here (blue dashed line) the projected 95% CL exclusion limit at the $\sqrt{s} = 14$ TeV LHC for $\mathcal{L} = 100$ fb^{-1}, as estimated in [55]. Naturally, the allowed flavor dependence is this higher mass range is even larger.

4.2 $\widetilde{\ell}_L\widetilde{W}$ models

We now assume that only the Winos and left-handed sleptons are light. The light spectrum is given by nearly degenerate, Wino-like chargino and neutralino, as well as charged sleptons and sneutrinos. Unlike the previous model, here the sneutrinos play a role in both the dipole amplitudes and in the LHC processes of interest, and we will assume that the masses of the charged sleptons and sneutrinos are very close, with mass-squared differences less than M_W^2, as is the case in the MSSM.

The dipole amplitudes are again quite simple, with the chirality flip occurring on the external fermion line(s). The expressions can be obtained from eqs. (4.1), (4.2) with $\alpha_Y \to \alpha_2$,

$$A_L = (A_L^{n_1})_{\mathrm{SU}(2)} + (A_L^{c_1})_{\mathrm{SU}(2)}\,, \qquad A_R \simeq 0\,, \tag{4.3}$$

$$\Delta a_\mu = \left(\Delta a_\mu^{n_1}\right)_{\mathrm{SU}(2)} + \left(\Delta a_\mu^{c_1}\right)_{\mathrm{SU}(2)}\,, \qquad d_e \simeq 0\,. \tag{4.4}$$

Again, the LHC signatures of these models are largely determined by the identity of the LSP, and by the mass splitting between the LSP and NLSP. Thus for example, for an LSP neutralino and an almost degenerate NLSP chargino, chargino masses up to $\sim 300 - 500$ GeV are excluded as the chargino-neutralino mass difference varies between $\sim 160 - 140$ MeV by searches for disappearing tracks [56].

Slepton pair production followed by decays to leptons plus Winos was recently studied in these models in [55], by recasting the ATLAS analysis [4]. In figure 3, we show the estimates of [55] for the region excluded by current LHC data (light-blue area), and for the reach of the 14 TeV LHC (dashed line), assuming a flavor-blind slepton spectrum, for different choices of the Wino mass M_2 and the common slepton mass m_L. We also plot the upper bounds on δ^{21}_{LL} (left) and δ^{32}_{LL} (right), and the LEP limit, $m_{\widetilde{\chi}_1^\pm} > 103$ GeV (assuming $m_{\widetilde{\chi}_1^0} = m_{\widetilde{\chi}_1^\pm} = M_2$). The present LHC exclusion, as estimated in [55], is stronger than in the Bino-LSP case, because of the larger number of production modes (such as sneutrino-slepton and sneutrino-sneutrino), that can lead to dilepton events. As for the LFV processes, as we can see from figure 3, a novel feature of this model is the possibility

JHEP10(2015)043

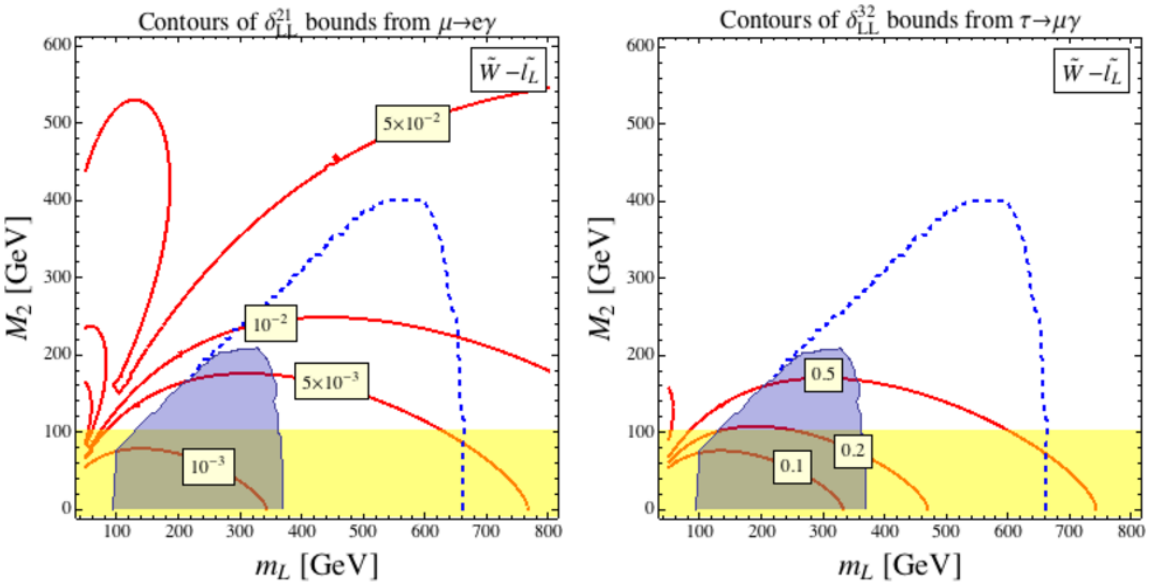

Figure 3. Upper limits on δ_{LL}^{21} (left) and δ_{LL}^{32} (right) in the plane $(m_L,\ M_2)$ for the model $\widetilde{\ell}_L\widetilde{W}$. The yellow region refers to the LEP exclusion. The light-blue area (dashed line) represents the current (future) LHC exclusion, as estimated in [55].

of cancellations between the two contributions to A_L, cf. eq. (4.3). This occurs for $m_L \approx 1.5 \times M_2$, for which the LSP is a sneutrino. However, for the region of parameter space probed by current LHC lepton plus missing energy searches, the allowed flavor dependence is more constrained than in the $\widetilde{\ell}_L\widetilde{B}$ model.

Finally, $(g-2)_\mu$ is non-zero in this model, because of the chargino contribution (see eq. (4.4)). However, the resulting Δa_μ is numerically negligible, due to the partial cancellation between the chargino and neutralino contributions and, more importantly, the absence of any $\tan\beta$ enhancement.

4.3 $\widetilde{\ell}_L\widetilde{B}\widetilde{W}$ models

These models combine all the superpartners considered so far: the left handed sleptons, the charged and neutral Winos, and the Bino. The right handed sleptons as well as the Higgsinos are assumed to be heavy, and we therefore neglect Bino-Wino mixing. As a result, it is again straightforward to compare the results of LHC lepton-based searches to CLFV constraints: the spectrum is completely specified by the left-handed slepton masses, which with no flavor dependence are given by m_L, the common Wino mass M_2 (up to possible small splittings), and the Bino mass M_1, and, given the absence of Higgsinos and LR slepton mixing, only diagrams with the chirality flip occurring on the external legs contribute,

$$A_L = (A_L^{n_1})_{U(1)} + (A_L^{n_1})_{\mathrm{SU}(2)} + (A_L^{c_1})_{\mathrm{SU}(2)}\,, \qquad A_R \simeq 0\,, \tag{4.5}$$

$$\Delta a_\mu = \left(\Delta a_\mu^{n_1}\right)^L_{U(1)} + \left(\Delta a_\mu^{n_1}\right)_{\mathrm{SU}(2)} + \left(\Delta a_\mu^{c_1}\right)_{\mathrm{SU}(2)}\,, \qquad d_e \simeq 0\,, \tag{4.6}$$

with no μ or $\tan\beta$ dependence.

JHEP10(2015)043

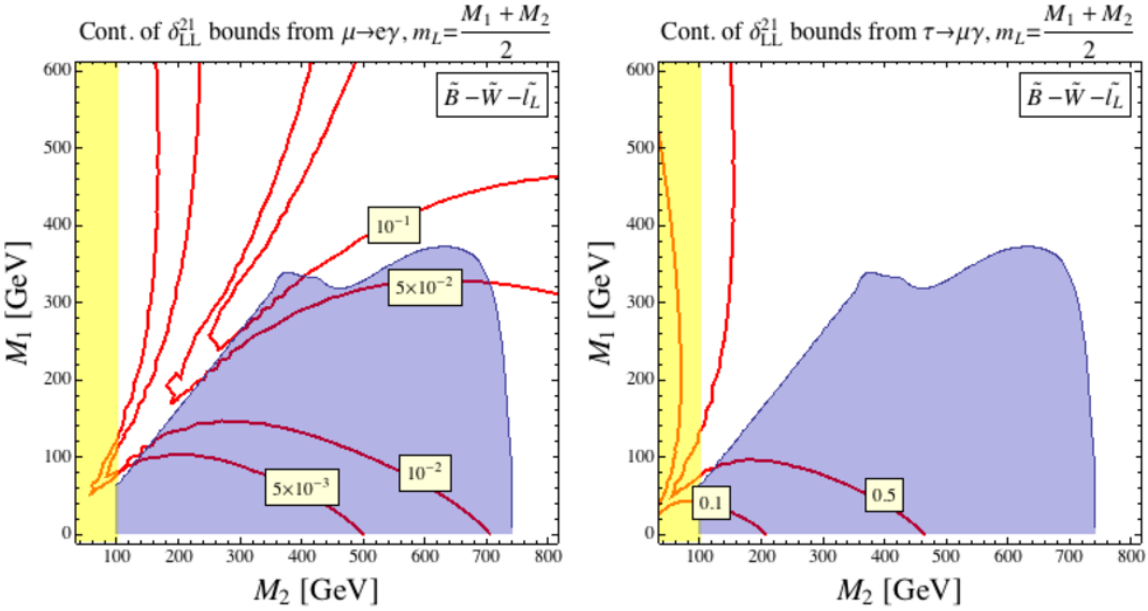

Figure 4. Upper limits on δ^{21}_{LL} (left) and δ^{32}_{LL} (right) in the plane $(M_2,\ M_1)$ for the model $\widetilde{\ell}_L\widetilde{B}\widetilde{W}$ assuming $m_L = (M_1 + M_2)/2$. The light-blue area is excluded by the CMS [6] direct search, the yellow region refers to the LEP exclusion.

At the same time, this model features a rich chargino-neutralino sector, and it has been employed by the LHC collaborations for the interpretation of searches based on multi-leptons plus missing energy [3, 6], assuming a Bino LSP, and sleptons half-way between the Bino and Wino. The highest sensitivity is reached in the case of heavy neutralino-chargino associated production, followed by decays to the Bino LSP through intermediate on-shell sneutrinos and sleptons. This decay chain leads to three-lepton events, with two OSSF leptons. In figure 4, we plot the upper bounds on δ^{21}_{LL} (left) and δ^{32}_{LL} (right) in the plane $(M_2,\ M_1)$ with the left-handed slepton mass taken at the value $m_L = (M_1 + M_2)/2$, which maximizes the LHC reach in the three-leptons plus missing transverse momentum channel. As we can see, Wino-like neutralino/chargino masses are excluded by CMS up to 700 GeV for LSP masses below roughly 300 GeV [6]. On the other hand, the CLFV constraints are relatively mild in this entire region: there is essentially no bound from $\tau \to \mu\gamma$, and δ^{21}_{LL} of few to 10% is allowed for the highest masses probed by the CMS search. These mild constraints are a consequence of a cancellation occurring between U(1) and SU(2) contributions in eq. (4.5), which feature opposite signs. In fact, for the value we chose for m_L, the two contributions exactly cancel when $M_1 \approx M_2$.

Finally, since the only chirality flip is on the external fermion leg(s), there is no contribution to the electron EDM. However, Δa_μ can be induced but only at negligible levels, as in the $\widetilde{\ell}_L\widetilde{W}$ model, because of partial cancellations of chargino and neutralino contributions and because there are no $\tan\beta$-enhanced contributions.

JHEP10(2015)043

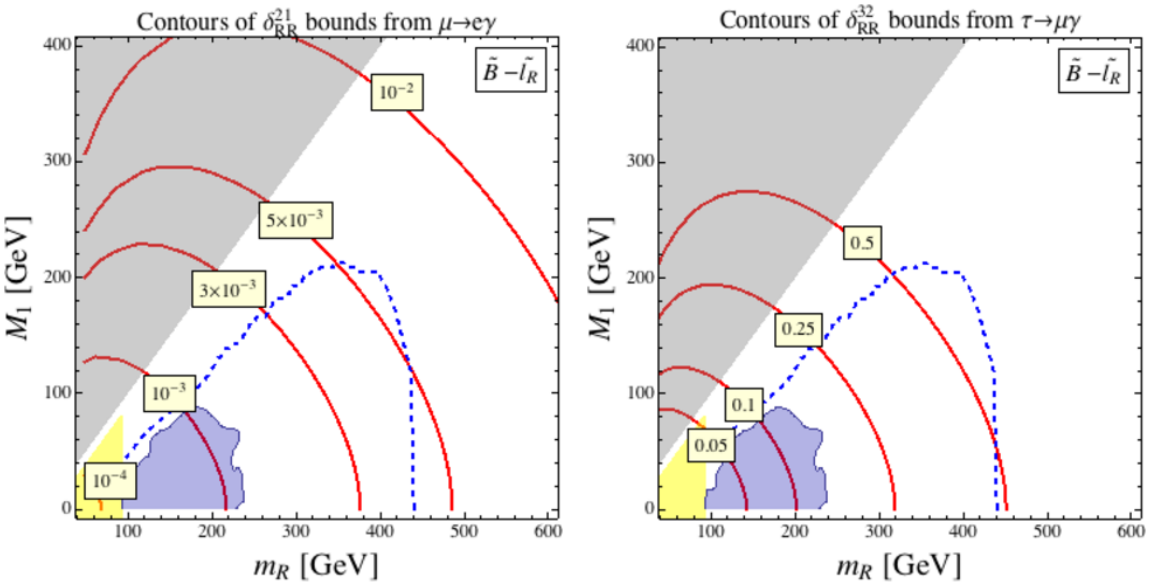

Figure 5. Upper limits on δ^{21}_{RR} (left) and δ^{32}_{RR} (right) in the plane $(m_R,\ M_1)$ for the model $\widetilde{\ell}_R\widetilde{B}$. The light-blue area is excluded by the ATLAS [1] direct search, the yellow region refers to the LEP exclusion while in the grey area the LSP is not neutral. The dashed line refers to the future LHC limit with $\sqrt{s} = 14\,\text{TeV}$ and $\mathcal{L} = 100\ \text{fb}^{-1}$, as estimated in [55].

4.4 $\widetilde{\ell}_R\widetilde{B}$ models

We now turn to models in which the light sleptons are right-handed, with the left-handed sleptons decoupled. The simplest of these contains just the Bino, in addition to the right handed sleptons. Our discussion will be brief here, since it is essentially the same as the discussion of the $\widetilde{\ell}_L\widetilde{B}$ model.

The simplified expressions for $A_{L,R}$, Δa_μ, and d_e can be obtained from eqs. (4.1), (4.2), with $L \leftrightarrow R$, and $\alpha_Y \to 4\alpha_Y$,

$$\begin{aligned} A_R &= (A_R^{n_1})_{U(1)}\,, & A_L &\simeq 0\,, \\ \Delta a_\mu &= \left(\Delta a_\mu^{n_1}\right)^R_{U(1)}\,, & d_e &\simeq 0\,. \end{aligned} \tag{4.7}$$

As in the $\widetilde{\ell}_L\widetilde{B}$ model, the electron EDM d_e vanishes, and Δa_μ is always negative and very small. In figure 5, we show contours of the upper bounds on the dimensionless MI parameter $\delta^{21}_{RR} \equiv \Delta^{21}_{RR}/m_R^2$ (left) and $\delta^{32}_{RR} \equiv \Delta^{32}_{RR}/m_R^2$ (right) in the $(m_R,\ M_1)$ plane.

As already anticipated, the CLFV constraints are stronger than in the $\widetilde{\ell}_L\widetilde{B}$ model, because of the larger hypercharge of the right-handed sleptons. On the other hand, the cross-section for Drell-Yan production of left-handed slepton is larger than for right handed sleptons, resulting in a lower sensitivity to the latter.

The discussion of this section carries over trivially to $\widetilde{\ell}_R\widetilde{B}\widetilde{W}$ models. Since the right-handed sleptons do not couple to pure Winos, the latter have no effect on either LHC slepton production or on the dipole amplitudes.

Models with only right-handed sleptons and Winos are somewhat special, predicting, in particular, no dipole amplitudes. We will briefly comment on such "exotic" models at the end of this section.

JHEP10(2015)043

4.5 $\widetilde{\ell}_L\widetilde{\ell}_R\widetilde{B}$ models

Models with both left-handed and right-handed sleptons are qualitatively different from the scenarios discussed above due to the possibility of left-right mixing, which allows for a chirality flip on the slepton line, and therefore a significant enhancement of the dipole amplitudes. As a result, analyzing the reach of LHC searches together with CLFV observables is trickier in this case. Even a relatively small left-right mixing, which has little effect on the slepton masses, and therefore on LHC observables, can significantly alter the predictions for the CLFV transitions. We also note that d_e does not vanish here, since the relevant diagrams involves the couplings of the two different fermion chiralities, and these are generically independent complex numbers. Finally, because of the enhancement mentioned above, large contribution to $(g-2)_\mu$ are possible, as we will see shortly.

The various dipole amplitudes are now given by,

$$A_L = (A_L^{n_1})_{U(1)} + (A_L^{n_3})_{U(1)}\,, \qquad A_R = (A_R^{n_1})_{U(1)} + (A_R^{n_3})_{U(1)}\,, \tag{4.8}$$

$$\Delta a_\mu = \left(\Delta a_\mu^{n_1}\right)^L_{U(1)} + \left(\Delta a_\mu^{n_1}\right)^R_{U(1)} + \left(\Delta a_\mu^{n_3}\right)_{U(1)}\,, \tag{4.9}$$

$$d_e = (d_e^{n_3})_{U(1)}\,. \tag{4.10}$$

While the amplitudes $(A_M^{n_1})_{U(1)}$, with $M = L, R$, involve only left handed or right handed sleptons, $(A_M^{n_3})_{U(1)}$ are proportional to the left-right mixing, which can in principle involve either same-generation, or different generation sleptons.

In figure 6, we show the bounds on the MIs $\delta^{21}_{RL} = \delta^{21}_{LR}$ (left) and $\delta^{32}_{RL} = \delta^{32}_{LR}$ (right) in the plane $(m_L = m_R,\ M_1)$. Note that we assume here degenerate left-handed and right-handed sleptons, in order to allow for a direct comparison with LHC search results. As before, the light-blue area highlights the exclusion set by the ATLAS analysis in [1] on smuon and selectron masses. As a reference, we also show the $\sqrt{s} = 14\,\text{TeV}$ LHC forecast as estimated for the $\widetilde{\ell}_L\widetilde{B}$ model in [55].[6]

We now turn to discuss contributions with LL and RR flavor-violating insertions, with the chirality flip coming from LR mixing of same-generation sleptons. Treating the LR mixing as an insertion, we will again show our results in the $(m_L = m_R,\ M_1)$ plane. This is of course an approximation, since the LR mixing necessarily implies a splitting of the two masses. However, as discussed above, even a small LR mixing, which has little effect on the masses, can significantly alter the dipole operators. In the following, we will also assume that the slepton A-terms are small, so that the left-right slepton mixing is proportional to $\mu\tan\beta$. The left-right mixings in the different generations are then correlated (and proportional to the relevant lepton mass). Furthermore, they are also correlated with the Higgsino masses, which are $\sim \mu$ for large μ. It is important to bear in mind however that these relations need not hold generally, for example, if some A-terms are large, or if additional parameters enter the Higgsino spectrum.

With these assumptions, the CLFV amplitudes, as well as $g-2$, are proportional to $|\mu\tan\beta|$. Motivated by $g-2$, in figure 7 (left) we show the contours of δ^{21}_{RR} and δ^{21}_{LL} for $\mu = 1\,\text{TeV}$ and $\tan\beta = 30$. It is easy to reinterpret the CLFV bounds for different choices of these parameters: roughly, the bounds on δ^{ij}_{RR} and δ^{ij}_{LL} scale as $(30\ \text{TeV})/(\mu\times\tan\beta)$.

[6] Note however that this estimate assumes the presence of left-handed sleptons only.

JHEP10(2015)043

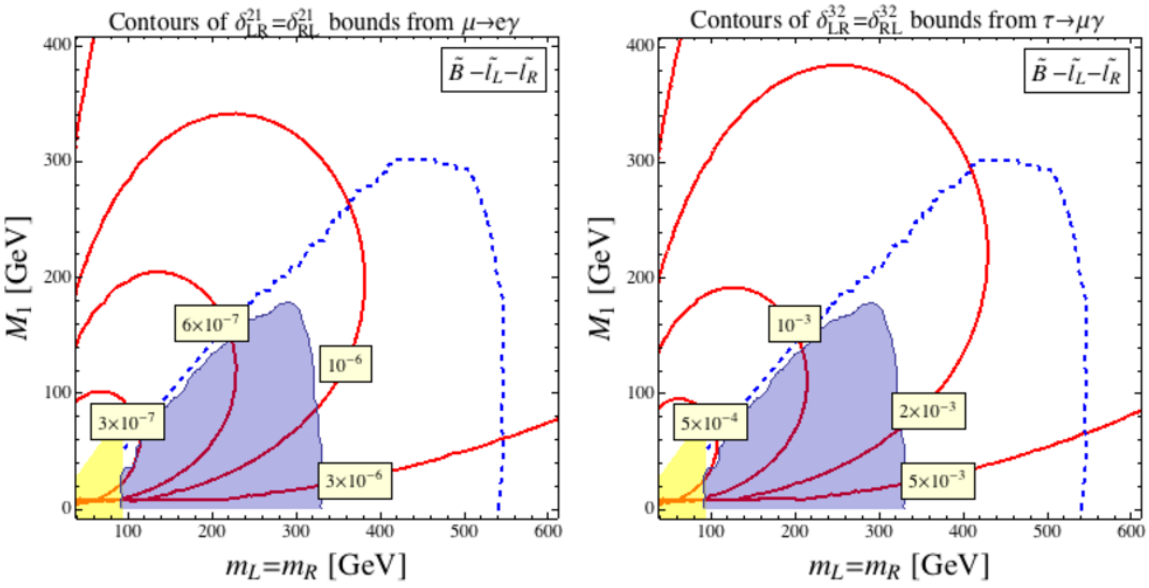

Figure 6. Upper limits on $\delta^{21}_{RL} = \delta^{21}_{LR}$ (left) and $\delta^{32}_{RL} = \delta^{32}_{LR}$ (right) in the plane $(m_L = m_R,\ M_1)$ for the model $\widetilde{\ell}_L\widetilde{\ell}_R\widetilde{B}$. The light-blue area is excluded by the ATLAS [1] direct search, the yellow region refers to the LEP exclusion. The dashed line refers to the future LHC limit with $\sqrt{s} = 14\,\text{TeV}$ and $\mathcal{L} = 100\ \text{fb}^{-1}$, as estimated in [55].

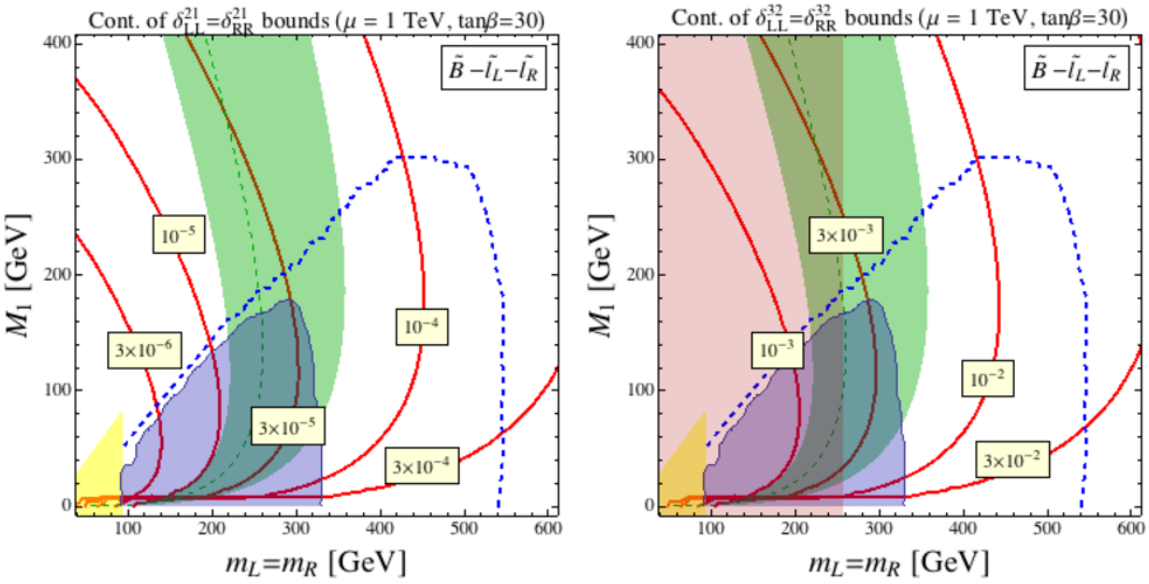

Figure 7. Upper limits on $\delta^{21}_{LL} = \delta^{21}_{RR}$ (left) and $\delta^{32}_{LL} = \delta^{32}_{RR}$ (right) in the plane $(m_L = m_R,\ M_1)$ for $\widetilde{\ell}_L\widetilde{\ell}_R\widetilde{B}$ models assuming $\mu = 1\,\text{TeV}$ and $\tan\beta = 30$. The light-blue area is excluded by the ATLAS [1] direct search, the yellow region refers to the LEP exclusion. The dashed line refers to the future LHC limit with $\sqrt{s} = 14\,\text{TeV}$ and $\mathcal{L} = 100\ \text{fb}^{-1}$, as estimated in [55]. The green band accounts for the muon $g-2$ anomaly at the 2σ level: $\Delta a_\mu = (2.9 \pm 1.8) \times 10^{-9}$. The red-shaded area is excluded by stau sector constraints (see text for details). The constraints on the δ's scale as $(30\ \text{TeV})/(\mu \times \tan\beta)$.

JHEP10(2015)043

Compared to the previously discussed models $\widetilde{\ell}_L\widetilde{B}$ and $\widetilde{\ell}_R\widetilde{B}$, we see that now, while the LHC bounds are only slightly more constraining, the bounds on the MIs are much more stringent. As a result, the present LHC direct exclusion is comparable with the limit from $\mu \to e\gamma$ only for values of the MIs $\delta^{21}_{LL} = \delta^{21}_{RR} \lesssim 10^{-4}$, $\delta^{21}_{LR} = \delta^{21}_{RL} \lesssim 10^{-6}$. Larger values of these LFV parameters would imply that the model is already excluded by MEG way beyond the reach of the LHC.

As mentioned above, an interesting feature of these models is that they can provide a supersymmetric contribution to Δa_μ with the right sign to reduce the tension between theoretical prediction and experiment. This is clearly seen in figure 7, where the green band corresponds to $\Delta a_\mu = (2.9 \pm 1.8) \times 10^{-9}$, thus accounting for the $(g-2)_\mu$ anomaly at the 2σ level or better.

Similarly, the right panel of figure 7 displays the bounds on δ^{32}_{RR} and δ^{32}_{LL}. However, the interpretation of the parameters in the smuon-stau system is a bit more subtle. Since the LR slepton mixing is proportional to the lepton mass, a large $\mu \tan\beta$ can have a significant effect on the stau mass eigenvalues, lowering the mass of the lightest combination. Thus, m_L and m_R stand for the smuon masses as before, while the stau masses are in general different as a result of the LR mixing. Furthermore, for given values of m_L and m_R, the LEP bound on the stau mass, $m_{\tilde{\tau}_1} \gtrsim 80\,\text{GeV}$ implies an upper bound on $|\mu \tan\beta|$.[7] An even stronger constraint follows from the condition of (meta)stability of the vacuum, since a large Higgs-stau-stau trilinear coupling in the potential can induce a charge-breaking minimum which is deeper than the correct electroweak breaking minimum. This implies the following bound [58–61]:

$$|\mu \times \tan\beta| \lesssim 39(\sqrt{m_L} + \sqrt{m_R})^2 - 10 \text{ TeV}. \tag{4.11}$$

The resulting excluded area is shaded in red.

The portion of the plane favoured by $(g-2)_\mu$ can be easily enlarged to values of the SUSY masses above the present and future LHC reach by increasing $|\mu \tan\beta|$. However, this would imply a much stronger constraint on LFV in the $\mu - e$ sector, as well as a stau spectrum heavier than selectrons and smuons to overcome the meta-stability bound of eq. (4.11): this is shown in the right panel of figure 7, where we see that for degenerate staus and sleptons the stau sector constraints partly exclude the region favoured by $(g-2)_\mu$.

Finally, let us comment on the electron EDM. Clearly, for the large values of $g-2$ considered here, an $\mathcal{O}(1)$ phase of μM_1 would be a phenomenological disaster. This is the well-known SUSY CP-problem: the new experimental limit $d_e < 8.7 \times 10^{-29}$ e cm [42] requires $\arg(\mu M_1)$ at the level of 10^{-4} or less.

4.6 $\widetilde{\ell}_L\widetilde{\ell}_R\widetilde{W}$ models

In these scenarios, the Higgsinos and Bino are decoupled while the Winos, and left- and right-handed sleptons are light. Since the Wino couples only to left-handed sleptons, the low-energy predictions of this model are the same as those of the previous simplified model

[7] LHC searches for direct EW production of staus have not reached the sensitivity yet to set a stronger bound. See e.g. [57].

JHEP10(2015)043

$\widetilde{\ell}_L\widetilde{W}$, eqs. (4.3), (4.4). As in some previous cases, LHC searches have not been interpreted yet in this simplified scenario. Nevertheless, given the presence of the left-handed sleptons, we expect them to be at least as stringent as in the case of model $\widetilde{\ell}_L\widetilde{W}$.

To summarize, the right-handed slepton plays a subdominant role and the phenomenology of this model is also captured by figure 3.

4.7 $\widetilde{\ell}_L\widetilde{B}\widetilde{H}$ models

We now turn to light Higgsino scenarios, starting with examples in which the only light fields are the left-handed sleptons, the Higgsinos and the Bino. The resulting amplitudes are:

$$A_L = (A_L^{n_1})_{U(1)} + (A_L^{n_2})_{\mathrm{U}(1)}\,, \qquad A_R \simeq 0\,, \tag{4.12}$$

$$\Delta a_\mu = \left(\Delta a_\mu^{n_1}\right)^L_{\mathrm{U}(1)} + \left(\Delta a_\mu^{n_2}\right)^L_{\mathrm{U}(1)}\,, \qquad d_e = (d_e^{n_2})^L_{\mathrm{U}(1)}\,. \tag{4.13}$$

In addition to the three scales m_L, M_1 and μ, these amplitudes are sensitive to $\tan\beta$. The dominant contribution is typically from the Bino-Higgsino diagrams of $(A_L^{n_2})_{\mathrm{U}(1)}$, which are proportional to the Bino-Higgsino mixing $\sim \mu\tan\beta$. Thus, for large $\tan\beta$, Δa_μ can account for the current anomaly if $\mu > 0$. In the following, we choose $\mu > 0$, $\tan\beta = 50$ to maximize Δa_μ. Since the leading contributions to the $\ell_i \to \ell_j\gamma$ amplitudes scale as $\mu\tan\beta$, the CLFV bounds we derive below can easily be reinterpreted for lower values of $\tan\beta$. Thus for example, for $\tan\beta = 5$, these bounds will weaken by one order of magnitude.

As for the mass scales involved, we examine two benchmark scenarios. In the first, $M_1 = \mu$, so that the light neutralino is a Bino-Higgsino mixture. In the second, M_1 and μ vary independently with $m_L = (M_1 + \mu)/2$, in analogy with the previous models we considered.

In the top panels of figure 8, we plot the upper bounds on δ^{21}_{LL} (left) and δ^{32}_{LL} (right) in the plane $(m_L,\ M_1 = \mu)$. The green band highlights the region preferred by the muon $g-2$: $\Delta a_\mu = (2.9\pm1.8)\times10^{-9}$. The ATLAS exclusion (light-blue area) and the future LHC prospects (dashed line) are the same as in the $\widetilde{\ell}_L\widetilde{B}$ models, and are based on slepton pair production followed by their decay into the (Bino component of the) neutralino LSP.[8] We also show in yellow the LEP exclusion on Higgsino-like charginos. We see that the LFV bounds are quite stringent in this case. In the region probed by the LHC lepton-based searches, $\delta^{21}_{LL} < 10^{-4}$ and $\delta^{32}_{LL} < 10^{-2}$.

In the bottom panels of figure 8, we show the results for the second slice of the parameter space we chose: independent μ and M_1 with intermediate sleptons, $m_L = (M_1+\mu)/2$. LHC searches can only probe these models for M_1 and μ which are sufficiently different, with the LSP being either a Bino or a neutral Higgsino depending on the hierarchy of M_1 and μ. While the low-energy constraints are similar to the previous case, the most sensitive searches at the LHC are based on Higgsino-like neutralino pair production. The subsequent decay of the Higgsinos into the intermediate sleptons induces events with 4 leptons and missing energy. Notice that such a decay preferably occur through the small

[8] Further constraints from lepton based-searches could arise from sneutrino production followed by decays into leptons plus Higgsino-like charginos.

JHEP10(2015)043

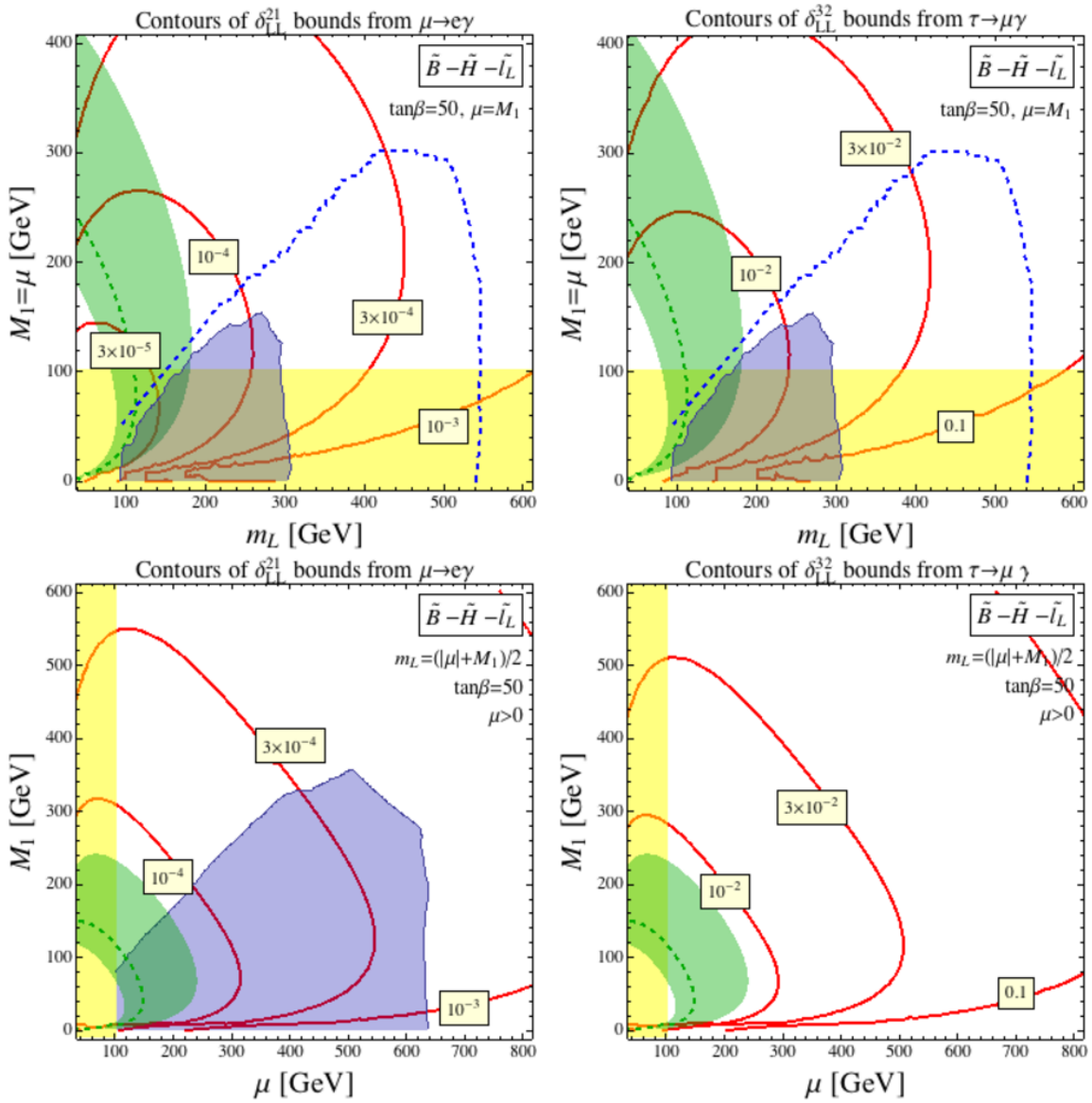

Figure 8. Upper limits on δ^{21}_{LL} (left) and δ^{32}_{LL} (right) for the model $\widetilde{\ell}_L\widetilde{B}\widetilde{H}$ in the $(m_L,\ M_1=\mu)$ plane (top panels) and in the $(\mu,\ M_1)$ plane with $m_L=(M_1+\mu)/2$ (bottom panels), for $\tan\beta=50$. The light-blue areas are excluded by ATLAS searches (see text for details), the yellow region shows the LEP exclusion. The dashed line refers to the future LHC limit with $\sqrt{s}=14\,\text{TeV}$ and $\mathcal{L}=100\ \text{fb}^{-1}$, as estimated in [55]. The green band accounts for the muon $g-2$ anomaly at the 2σ level: $\Delta a_\mu=(2.9\pm1.8)\times10^{-9}$. For lower $\tan\beta$, the constraints on the δ's weaken by a factor $50/\tan\beta$.

gaugino components of the heavier neutralinos, hence it is still democratic for the e and μ flavors. On the other hand, the Higgsinos would prefer to decay into staus, if kinematically accessible, especially for large $\tan\beta$. Therefore, if the only light sleptons are the selectron and the smuon, we can use the 4-lepton ATLAS search [5] to constrain these models (see bottom left panel of figure 8). However, if the stau is light too, the branching fractions

JHEP10(2015)043

of Higgsino decays to selectrons and smuons will be very small. Such scenarios are still constrained by the LEP bound (see bottom right panel of figure 8). Additional constraints can be extracted from LHC searches for associate production of charginos and neutralinos decaying to intermediate staus, leading to events with three taus and missing energy [57]. For a light LSP, this search can set a limit on the Higgsino mass up to 350 GeV [62].

Finally, notice that this model features a non-vanishing contribution to d_e. As discussed above for the model $\widetilde{\ell}_L \widetilde{\ell}_R \widetilde{B}$, present bounds then require a certain suppression of the flavor-blind phase $\arg(\mu M_1)$.

4.8 $\widetilde{\ell}_R \widetilde{B} \widetilde{H}$ models

In this scenario, the left-handed sleptons and Winos are heavy while the right-handed sleptons, the Higgsinos and the Bino are light. The amplitudes can be obtained by exchanging $R \to L$ in the previous model,

$$A_R = (A_R^{n_1})_{\mathrm{U}(1)} + (A_R^{n_2})_{\mathrm{U}(1)}\,, \qquad A_L \simeq 0\,, \tag{4.14}$$

$$\Delta a_\mu = \left(\Delta a_\mu^{n_1}\right)^R_{\mathrm{U}(1)} + \left(\Delta a_\mu^{n_2}\right)^R_{\mathrm{U}(1)}\,, \qquad d_e = (d_e^{n_2})^R_{\mathrm{U}(1)}\,. \tag{4.15}$$

However, in this case, $\mu < 0$ is required in order to account for the muon $g-2$ anomaly. As before, we maximize these contributions by choosing $\tan\beta = 50$, keeping in mind that the CLFV bounds scale as $\tan\beta$. The resulting bounds on δ^{21}_{RR} (left) and δ^{32}_{RR} (right) are shown in figure 9 for two benchmark scenarios in complete analogy to the $\widetilde{\ell}_L \widetilde{B} \widetilde{H}$ models: $(m_R,\ M_1 = -\mu)$ (top panels) and $(\mu,\ M_1)$ with $m_R = (M_1 + \mu)/2$ (bottom panels). Note that the low-energy bounds are somewhat stronger than those of figure 8, because of the larger hypercharge of the right-handed sleptons. The discussion of the LHC searches for $\widetilde{\ell}_L \widetilde{B} \widetilde{H}$ carries over to this case as well. We only note that in the top-panel plots of figure 8 we employed the same search as in figure 9 and, in this case, we do not expect significant constraints from other searches, given the absence of sneutrinos.

4.9 $\widetilde{\ell}_L \widetilde{W} \widetilde{H}$ models

The last class of models we discuss in detail has left-handed sleptons, Higgsinos and Winos. Only the right-handed sleptons and Bino are decoupled. The particle content of these models is rich, with three neutralinos, two charginos, as well as charged and neutral sleptons. Several diagrams therefore contribute to the dipole amplitudes,

$$A_L = (A_L^{n_1})_{\mathrm{SU}(2)} + (A_L^{c_1})_{\mathrm{SU}(2)} + (A_L^{n_2})_{\mathrm{SU}(2)} + (A_L^{c_2})_{\mathrm{SU}(2)}\,, \qquad A_R \simeq 0\,, \tag{4.16}$$

$$\Delta a_\mu = \left(\Delta a_\mu^{n_1}\right)^L_{\mathrm{SU}(2)} + \left(\Delta a_\mu^{c_1}\right)^L_{\mathrm{SU}(2)} + \left(\Delta a_\mu^{n_2}\right)^L_{\mathrm{SU}(2)} + \left(\Delta a_\mu^{c_2}\right)^L_{\mathrm{SU}(2)}\,, \qquad d_e = (d_e^{c_2})_{\mathrm{SU}(2)} + (d_e^{n_2})_{\mathrm{SU}(2)}\,. \tag{4.17}$$

These are typically dominated by Wino-Higgsino diagrams, which are $\tan\beta$ enhanced. In particular, a large contribution to the muon $g-2$, from $\left(\Delta a_\mu^{c_2}\right)^L_{\mathrm{SU}(2)}$, is a pretty generic prediction of these scenarios. This can be clearly seen in figure 10, where we again plot the bounds on δ^{21}_{LL} (left) and δ^{32}_{LL} (right), for the simplifying choice $\mu = M_2$. The green band, corresponding to $\Delta a_\mu = (2.9 \pm 1.8) \times 10^{-9}$, is particularly wide, even for $\tan\beta = 20$.

JHEP10(2015)043

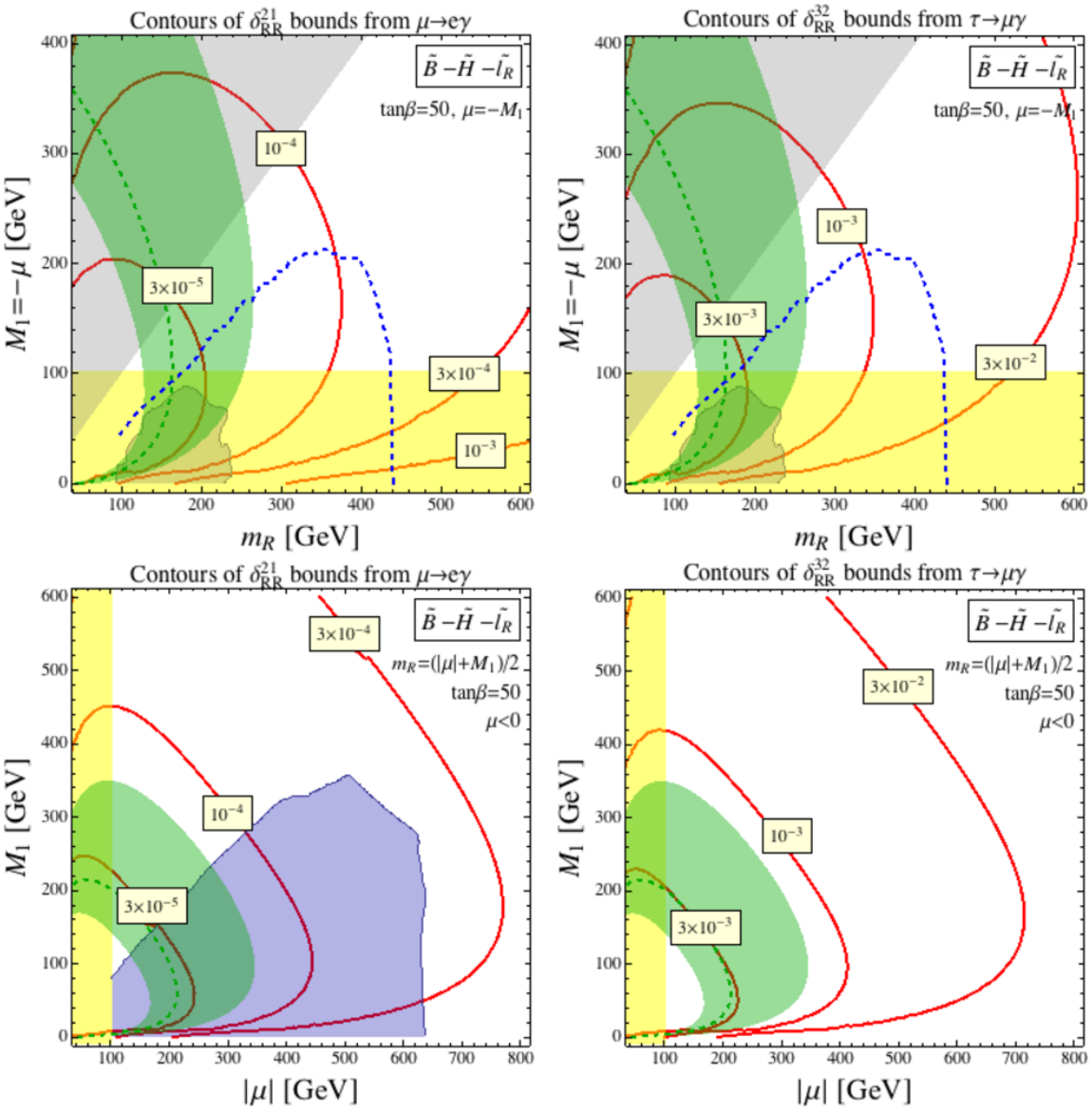

Figure 9. Upper limits on δ^{21}_{RR} (left) and δ^{32}_{RR} (right) for $\widetilde{\ell}_R\widetilde{B}\widetilde{H}$ models in the $(m_R,\ M_1=-\mu)$ plane (top panels) and in the $(\mu,\ M_1)$ plane with $m_R=(M_1+|\mu|)/2$ (bottom panels), for $\tan\beta=50$. is assumed. The light-blue areas are excluded by ATLAS searches (see the text for details), the yellow region refers to the LEP exclusion. The dashed line refers to the future LHC limit with $\sqrt{s}=14\,\text{TeV}$ and $\mathcal{L}=100\ \text{fb}^{-1}$, as estimated in [55]. The green band accounts for the muon $g-2$ anomaly at the 2σ level: $\Delta a_\mu=(2.9\pm1.8)\times10^{-9}$. For lower $\tan\beta$, the constraints on the δ's weaken by a factor $50/\tan\beta$.

The LHC exclusion is the same as in $\widetilde{\ell}_L\widetilde{W}$ models, since DY-produced selectrons and smuons still prefer decaying into a Wino-like neutralino. LFV constraints are also quite strong, again because of the $\tan\beta$ enhancement of Wino-Higgsino diagrams, although some cancellations are possible for $\mu=M_2\approx3m_L$.

JHEP10(2015)043

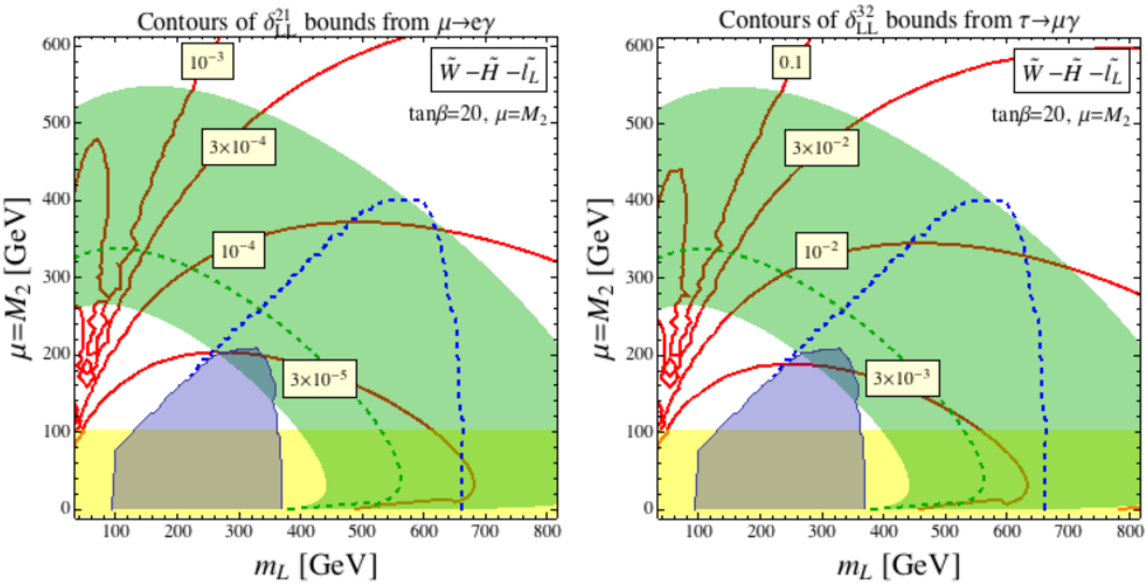

Figure 10. Upper limits on δ_{LL}^{21} (left) and δ_{LL}^{32} (right) for $\widetilde{\ell}_L\widetilde{W}\widetilde{H}$ models, in the $(m_L,\ M_2=\mu)$ plane for $\tan\beta = 20$. The light-blue area (dashed line) represents the current (future) LHC exclusion, with the latter taken from [55]. The yellow region refers to the LEP exclusion. The green band accounts for the muon $g-2$ anomaly at the 2σ level: $\Delta a_\mu = (2.9 \pm 1.8)\times 10^{-9}$. The bounds on the δ's scale with $\tan\beta$.

4.10 $\widetilde{\ell}_R\widetilde{W}$ models

Models in which only the right-handed sleptons and the Winos are light are somewhat special. Of course, if the Higgsinos, Bino, and left-handed sleptons were completely decoupled, the dipole transitions would vanish, and the right-handed sleptons would be long-lived. Realistically however, the leading contributions to dipole transitions arise from Wino/Bino mixing effects since the Bino couples to right-handed fields. In our setup, such mixings are roughly given by $\sim (m_Z^2 t_\beta^{-1})/(\mu M_1)$ and therefore very suppressed. As a result, all low-energy observables receive negligible effects.

As for collider searches, we note that the right-handed sleptons will still decay to the LSP, through the small Bino component. If such a mixing is suppressed enough, the decay could occur at a displaced vertex or even outside the detector. However, this would require super-heavy Bino and Higgsinos. In this case the relevant bound would come from charged track searches, as quoted at the beginning of the section. If on the contrary the decay is prompt, the constraints from direct LHC searches should resemble those of model $\widetilde{\ell}_R\widetilde{B}$. On the other hand, a Wino-like lightest neutralino corresponds to an almost degenerate chargino, and thus one has to take into account a lower bound on the spectrum from chargino searches at LEP: $M_2 \gtrsim 100\,\text{GeV}$.

4.11 Models with no light gauginos: $\widetilde{\ell}_L\widetilde{H}$, $\widetilde{\ell}_R\widetilde{H}$, $\widetilde{\ell}_L\widetilde{\ell}_R\widetilde{H}$

Models without light gauginos, as well as models with no Bino and only right-handed sleptons (like the previously discussed $\widetilde{\ell}_R\widetilde{W}$ and its possible extension $\widetilde{\ell}_R\widetilde{W}\widetilde{H}$), are of little

JHEP10(2015)043

interest for our discussion of the interplay between LFV observables and collider searches, since the low-energy processes are suppressed to negligible rates by small couplings of the Higgsinos to the sleptons. Nevertheless, they can have an interesting LHC phenomenology, as mentioned above for the $\widetilde{\ell}_R\widetilde{W}$ case. Further examples are provided in [55], where it is shown, for instance, that models like $\widetilde{\ell}_L\widetilde{H}$ can be constrained more strongly than $\widetilde{\ell}_L\widetilde{W}$, for certain choices of the parameters. These scenarios are better probed at collider experiments, with low-energy observables providing little sensitivity.

4.12 Heavy superpartner decoupling

Our results for the different simplified models can be taken at face value: we have used CLFV searches to constrain new particles with the quantum numbers of charged sleptons, gauginos and Higgsinos. Naturally however, in order to interpret these results in the context of supersymmetry, one must estimate the effects of the heavy superpartners which we omitted. This is especially relevant for the CLFV constraints, which generically fall off as the second power of the superpartner scale, while LHC cross sections fall much more steeply.

By comparing the different examples above we can get a qualitative estimate for the importance of different superpartners. The largest contributions involve either Higgsinos, or left-right slepton mixing. The former depends on $\mu \tan\beta$, and decouple as $M_1 \tan\beta/\mu$ for large μ. If Higgsinos are decoupled, and in the absence of LR slepton mixing, bounds on δ_{LL} are hardly affected by right-handed sleptons and vice-versa. This is the case in the first four models we discussed. Comparing the $\widetilde{\ell}_L\widetilde{B}\widetilde{W}$ models to the $\widetilde{\ell}_L\widetilde{B}$ or $\widetilde{\ell}_L\widetilde{W}$ models we can see that the effects of heavier Binos or Winos are small. As discussed above, the results are much more sensitive to heavier Higgsinos. Similarly, if the light sleptons are predominantly left handed, but with a small admixture of right handed sleptons, the CLFV constraints are sensitive to the heavier slepton states.

To estimate the importance of decoupled superpartners in each of the models, we vary the parameters m_L, m_R, M_1, M_2, μ and $\tan\beta$, and require that the CLFV amplitude used to derive the bounds above is at least 5 times larger than all other amplitudes. We note that this is a very strong requirement. The largest amplitudes are always the $\mu \tan\beta$ enhanced ones, coming from either Higgsino diagrams or from left-right slepton mixing. With no A-terms, both these effects are controlled by $\mu \tan\beta$, and cannot be disentangled. The conditions we find are collected in table 2.

5 Implications of LFV for LHC searches

We now turn to discuss the possible impact of slepton flavor dependence on different LHC searches. Specifically, we will only consider lepton plus missing energy searches in simplified models containing sleptons, Binos and Winos. We limit our discussion to models with sleptons of a single chirality and a neutralino LSP. To simplify notation, we therefore omit the chirality index of the sleptons. The basic production process, common to all of these models, is Drell-Yan slepton pair production, with each slepton decaying to one lepton and the LSP.

JHEP10(2015)043

model	region of validity
$\widetilde{\ell}_L\widetilde{B}$	For $M_1 \lesssim 150\,\text{GeV}$: $m_R \gtrsim 2\,\text{TeV}$ (i.e. $m_R/m_L \gtrsim 5 \div 10$), $M_2 \gtrsim 500\,\text{GeV}$ and $\mu \gtrsim 1\,\text{TeV}$ ($3\,\text{TeV}$ if $\tan\beta \gtrsim 10$) For $M_1 \gtrsim 300\,\text{GeV}$: $m_R \gtrsim 10\,\text{TeV}$ (i.e. $m_R/m_L \gtrsim 25$), $\mu \gtrsim 4\,\text{TeV}$ and $\tan\beta \lesssim 5$
$\widetilde{\ell}_L\widetilde{W}$	$M_2 \lesssim 180\,\text{GeV}$, $\tan\beta \lesssim 3$, $\mu \gtrsim 12\,\text{TeV}$ and $M_1 \gtrsim 3\,\text{TeV}$ or $m_R \gtrsim 2\,\text{TeV}$
$\widetilde{\ell}_L\widetilde{B}\widetilde{W}$	$\mu \gtrsim 2\,\text{TeV}$, $m_R \gtrsim 2\,\text{TeV}$ (i.e. $m_R/m_L \gtrsim 5 \div 10$)
$\widetilde{\ell}_R\widetilde{B}$	$m_L \gtrsim 2\,\text{TeV}$ (i.e. $m_L/m_R \gtrsim 5 \div 10$), $\mu \gtrsim 1\,\text{TeV}$ ($2.5\,\text{TeV}$ for $\tan\beta \gtrsim 10$)
$\widetilde{\ell}_L\widetilde{\ell}_R\widetilde{B}$	$\mu \gtrsim 500\,\text{GeV}$
$\widetilde{\ell}_L\widetilde{B}\widetilde{H}$	$M_2 \gtrsim 2\,\text{TeV}$
$\widetilde{\ell}_R\widetilde{B}\widetilde{H}$	$m_L/m_R \gtrsim 2$
$\widetilde{\ell}_L\widetilde{W}\widetilde{H}$	$m_R \gtrsim \mu/2$

Table 2. Region of validity of CLFV estimates for the different simplified models.

In some of the models, chargino-chargino, chargino-neutralino, or neutralino-neutralino pair production are possible too. These have a much higher reach compared to Drell-Yan production, because of the larger cross-sections. In the following we will discuss these different processes in turn.

Flavor-blind simplified models containing sleptons and neutralinos/charginos were analyzed by ATLAS and CMS. Since our aim is to estimate the effects of flavor dependence on these searches, we start by qualitatively reproducing the relevant exclusion for each of the flavor-blind models, and then repeat the analysis in the presence of some slepton mass splitting and/or mixing. We use CheckMATE [63] to reinterpret the searches.[9] We therefore concentrate on several ATLAS analyses which are incorporated and validated in CheckMATE. Signal events are generated using MadGraph5_aMC@NLO [69], with the showering performed by the PYTHIA package [70].

5.1 $\widetilde{\ell}_L\widetilde{B}$, $\ell = e, \mu$ models

In $\widetilde{\ell}_L\widetilde{B}$ models, sleptons are only produced via γ^*- or Z-mediated Drell-Yan processes. Since the slepton couplings to the photon and the Z are diagonal in the slepton mass basis, these processes result in $\widetilde{\ell}_i^+\widetilde{\ell}_i^-$ pairs with $i = 1, 2$, and flavor mixing has no effect on the production.[10] On the other hand, flavor mixing has an important role in slepton decays. In the presence of nonzero mixing, each slepton mass eigenstate can decay to the LSP in association with either an electron or a muon, so that slepton pair production leads to missing energy and $e^\pm\mu^\mp$ pairs, in addition to OSSF lepton pairs. This may affect the

[9] CheckMATE relies on several code packages and algorithms: the Delphes 3 detector simulation [64], the FastJet package [65, 66] which implements many sequential recombination algorithms (such as anti-k_T [67]), and the CLs prescription [68] for statistical discrimination.

[10] Note that flavor mixing could enter through LR Z coupling, but we neglect LR mixing throughout this section.

JHEP10(2015)043

sensitivity of searches based on OSSF leptons. Furthermore, Opposite Sign Different Flavor (OSDF) dileptons, specifically $e^{\pm}\mu^{\mp}$ pairs, are sometimes used in data-driven background estimates, with the assumption that the SUSY signal has no contribution in these channels.

We first reproduce the results of the ATLAS search for slepton pair production, based on final states with OSSF dileptons plus missing energy [1], assuming degenerate selectrons and smuons with no flavor mixing.[11] We apply a flat K-factor of 1.3 to the leading-order cross-section as calculated by MadGraph5, in order to reproduce the cross-section quoted in [1]. The excluded region in the slepton-LSP mass plane is displayed in figure 11(a). Note that the common slepton mass here coincides with m_L, and the LSP mass is given by M_1. The excluded region is color coded to indicate the most sensitive exclusion channel at each point. Thus for example, SR_mT$_2$_90_elel requires an electron-positron pair with stranverse mass [71, 72] above 90 GeV. As expected, the different models are excluded by the $e^{\pm}e^{\mp}$ and $\mu^{\pm}\mu^{\mp}$ channels. Note however, that the search [1] is sensitive to additional final states, since it also targets chargino pair production followed either by slepton-mediated chargino decays to leptons, or by gaugino-mediated decays to W's. The latter are important if the sleptons are heavy, and motivate SR_WWa, SR_WWb and SR_WWc (see legend of figure 11(a)) which target W pairs and missing energy. Slepton-mediated chargino decays on the other hand lead to OS dileptons and missing energy, with no correlation between the two lepton flavors. These channels motivate SR_mT$_2$_90_elmu and SR_mT$_2$_110_elmu, which involve $e^{\pm}\mu^{\mp}$ and mT$_2$ above 90 GeV and 110 GeV respectively, and will be relevant for our discussion below.

We now consider the possibility of flavor dependent slepton masses. As a first estimate of the allowed flavor parameters, we start from the low-energy bounds on δ^{21}_{LL} derived in the previous section using the MI approximation. Examining figure 2, we see that in the relevant region of the parameter space, the allowed values of δ^{21}_{LL} vary between $10^{-3} - 10^{-2}$. We can then translate these into allowed regions in the slepton masses and mixing. As noted above, the MI approximation fails for large relative mass splittings, so throughout this section we use the full expressions reported in the appendix to obtain the CLFV constraints on the slepton parameters.

In the limit of small mixings and large mass splittings, the cross-sections for selectron pair production and smuon pair production can be very different. Furthermore, since the efficiency of the search decreases as the slepton mass approaches the LSP mass, large slepton mass differences would result in different efficiencies for selectron and smuon discovery. The LHC signatures of such models are essentially the same however as in flavor-blind models: e^+e^- plus missing energy, and $\mu^+\mu^-$ plus missing energy. Thus, in this limit, the ATLAS analysis, which treats the ee and $\mu\mu$ samples separately, does more than place bounds on degenerate selectrons and smuons. Rather, it separately constrains the selectron mass and smuon mass. Indeed, this flavor information is displayed in the updated ATLAS analysis, which exhibits the separate limits on the selectron and smuon in the auxiliary plots [51].

[11] The more recent analysis [4] has been embedded into CheckMATE but has not been validated. Nevertheless, the updated limits are very similar to those employed here.

JHEP10(2015)043

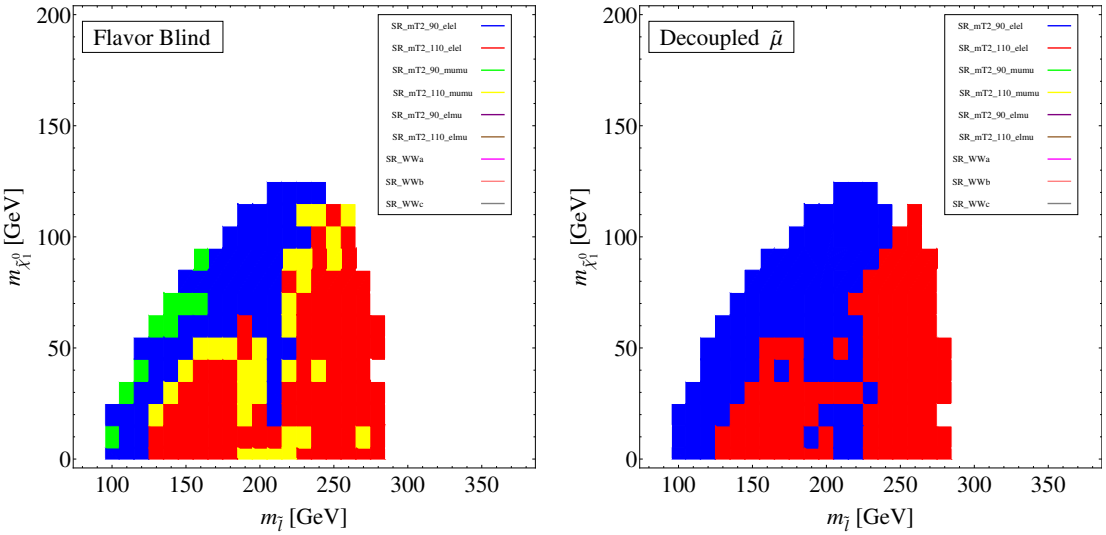

(a) Flavor blind: $\Delta m = 0$, $\sin 2\theta = 0$.

(b) Decoupled $\tilde{\mu}$, $\sin 2\theta = 0$.

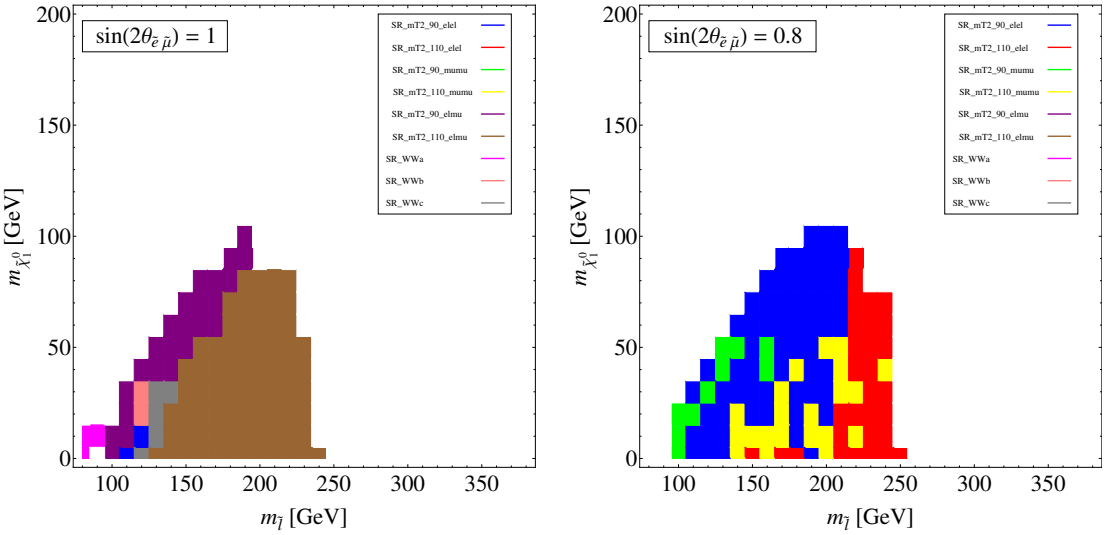

(c) Large mixing: small Δm, $\sin 2\theta = 1$.

(d) Large mixing: small Δm, $\sin 2\theta = 0.8$.

Figure 11. Reinterpreting the ATLAS analysis [1] to set limits on $\widetilde{\ell}_L\widetilde{B}$ models ($\ell = e, \mu$) with different assumptions about flavor: (a) degenerate sleptons with no mixing; (b) selectron only; (c), (d) almost degenerate sleptons with $\sin\theta = 1$ and $\sin\theta = 0.8$ respectively. $m_{\tilde{l}}$ denotes the common slepton mass in (a), (c), (d), and the selectron mass in (b). The excluded region is color-coded according to the most sensitive exclusion channel at each point (see legend).

For completeness, we illustrate this point by fixing the smuon mass at 400 GeV, well above the lower bounds of figure 11(a). We then use CheckMATE to reinterpret the ATLAS search [1] for models with different selectron and Bino masses. The results are shown in figure 11(b). As expected, the exclusion limit for the selectron remains virtually unchanged.

JHEP10(2015)043

In the opposite limiting case, the sleptons are almost degenerate, and large mixings are allowed. The production cross-sections of the two slepton mass eigenstates are practically equal. Thus, signal events redistribute among the ee, $\mu\mu$ and $e\mu$ final states with fractions

$$\begin{aligned} \frac{N(e^{\pm}\mu^{\mp})}{N(e^{+}e^{-})} &= \frac{\sin^2 2\theta}{\cos^4\theta + \sin^4\theta}\,, \\ N(\mu^{+}\mu^{-}) &\sim N(e^{+}e^{-})\,. \end{aligned} \tag{5.1}$$

Typically, searches based on just OSSF dileptons lose sensitivity in this scenario, with signal events "leaking" into $e^{\pm}\mu^{\mp}$ final states. However, as discussed above, the analysis of [1] is sensitive to $e^{\pm}\mu^{\mp}$ final states too. The modified limits obtained for maximal mixing, $\sin 2\theta = 1$, and for a mixing of $\sin 2\theta = 0.8$, are shown respectively in figure 11(c) and figure 11(d), assuming almost degenerate sleptons. Indeed, for the maximal mixing case the most sensitive exclusion channels are those involving $e\mu$ pairs, while for $\sin 2\theta = 0.8$ the OSSF channels are the dominant ones. Either way, the reach in the slepton mass is reduced by roughly 50 GeV compared to the flavor blind models, and the reach in the Bino mass goes down by about 40 GeV.

Naturally, some of the parameter space displayed in figure 11(c) and figure 11(d) is excluded by $\mu \to e\gamma$. In figure 12 we show this constraint (dark hatched region), for two values of the slepton mass splitting, $\Delta m = 5 \times 10^{-3}\, m_{\tilde{\ell}}$ (upper panels) and $\Delta m = 3 \times 10^{-3}\, m_{\tilde{\ell}}$ (lower panels). We also reproduce here the region excluded by the ATLAS data (light grey), corresponding to figures 11(c)), (11(d), as well as the original excluded region (dark grey) of the flavor-blind model as in figure 11(a).

For mass splittings of order the slepton widths, slepton flavor oscillations may be important [75, 76], and as the mass splitting becomes much smaller than the width, the fraction of $e^{\pm}\mu^{\mp}$ final states tends to zero. Specifically, the cross-section for slepton pair production followed by their decay to a final state with $e^{\pm}\mu^{\mp}$ and missing energy is given by [76],

$$\sigma_{e\mu}^{\text{pair}} = \sigma_0^{\text{pair}} \frac{\sin^2 2\theta}{2}\, r_\Gamma \tag{5.2}$$

where σ_0^{pair} denotes the cross section in the absence of flavor mixing, and r_Γ encodes the finite width effects,

$$r_\Gamma \equiv \frac{3x^2 + x^4}{(1+x^2)^2} \tag{5.3}$$

with $x \equiv \Delta m/\Gamma$. We verified that for the parameters of figure 12, $r_\Gamma \sim 1$ so that the finite width effects are very small.

We see that for $\Delta m = 5 \times 10^{-3}\, m_{\tilde{\ell}}$ with maximal mixing, LHC searches and $\mu \to e\gamma$ have comparable sensitivity to the models, while for all other choices, with smaller values of $\sin 2\theta \Delta m/m$, the LHC has better sensitivity. Finally, the reduced LHC sensitivity compared to the flavor-blind case is clearly seen in these plots.

5.2 $\widetilde{\ell}_R\widetilde{B}$, $\ell = e, \mu$ models

The discussion of the previous section carries over to this case as well, but the allowed flavor effects are milder. As can be seen in figure 5, the allowed δ^{12}_{RR} is at most one or two permille throughout the parameter space probed by current searches.

JHEP10(2015)043

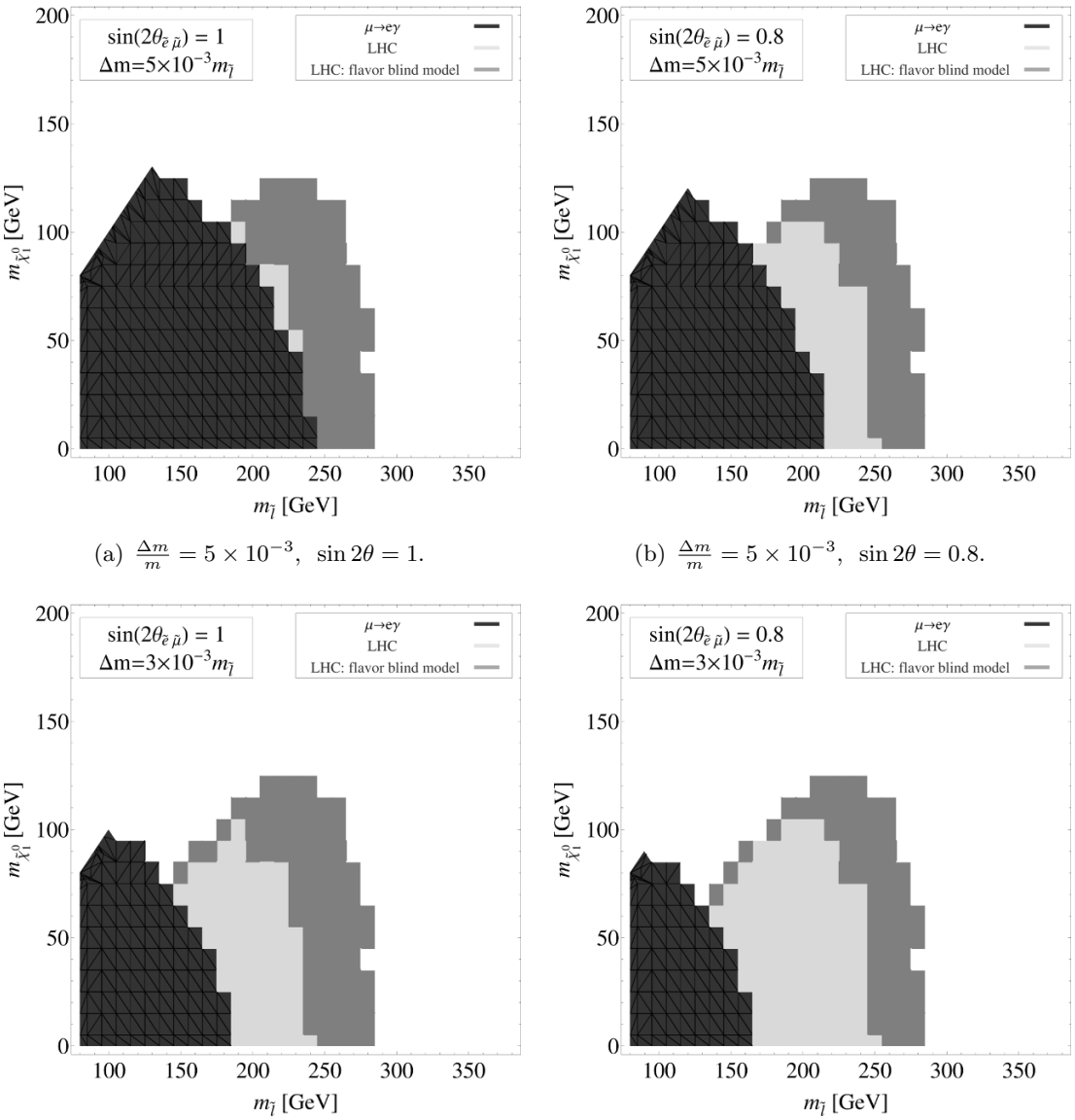

(a) $\frac{\Delta m}{m} = 5 \times 10^{-3}$, $\sin 2\theta = 1$.

(b) $\frac{\Delta m}{m} = 5 \times 10^{-3}$, $\sin 2\theta = 0.8$.

(c) $\frac{\Delta m}{m} = 3 \times 10^{-3}$, $\sin 2\theta = 1$.

(d) $\frac{\Delta m}{m} = 3 \times 10^{-3}$, $\sin 2\theta = 0.8$.

Figure 12. The excluded region (light grey), in the $m_{\tilde{\ell}} - m_{\chi}$ plane, obtained by reinterpreting the ATLAS analysis for almost degenerate sleptons (selectron-smuon) with relative mass splittings $\Delta m/m = 5 \times 10^{-3}$ (top) and $\Delta m/m = 3 \times 10^{-3}$ (bottom), for maximal mixing (left) and for $\sin 2\theta = 0.8$ (right). The dark grey indicates the excluded region of figure 11(a) (flavor blind sleptons) which is now allowed. The dark hatched region is excluded by $\mu \to e\gamma$.

For very small mixings and large mass differences, the ATLAS search yields separate bounds on the R selectron and smuon. For order-one mixings, the relative mass splittings has to be at the permille level because of the bound on δ^{12}_{RR}. However, the R-sleptons width is $\Gamma \lesssim 0.0045 \times m_R$. Thus, the fraction of $e\mu$ final states is damped by the small r_Γ. Flavor mixing effects will be relevant however at the 14 TeV LHC, since for the higher

JHEP10(2015)043

mass scales probed at 14 TeV, mass splittings larger than Γ are compatible with $\mu \to e\gamma$ (see figure 5).

5.3 $\widetilde{\ell}_L\widetilde{B}$, $\ell = \mu, \tau$ models

As can be seen in figure 2, very large flavor effects are possible in this case. We again distinguish between two limiting cases. With small stau-smuon mixing, $\mu^\pm\mu^\mp$ pairs plus missing energy have the same sensitivity to the smuon as in the flavor-blind scenarios. Large smuon-stau mixings on the other hand, lead to a smaller branching ratio for $\mu^\pm\mu^\mp$, with some slepton pairs decaying to opposite sign muons and taus, which largely escape detection (except possibly when the tau decays to a muon). However, the selectron in this case is constrained to be a pure state, and, if it is close in mass to the smuon, the searches are still sensitive to the selectron through e^+e^- plus missing energy channels.

5.4 $\widetilde{\ell}_L\widetilde{B}\widetilde{W}$ models

5.4.1 Limits from $\widetilde{\chi}^+\widetilde{\chi}^-$ production

Here the signature of interest is two opposite sign leptons plus missing energy, coming from chargino pair production, with each chargino decaying into a charged lepton, a neutrino, and the LSP, via either a slepton or a sneutrino. These channels were used to set limits on the models in [1], assuming six degenerate left-handed sleptons, $\widetilde{e}$, $\widetilde{\mu}$, $\widetilde{\tau}$ plus three sneutrinos, with mass halfway between the chargino and neutralino. The chargino was assumed to be 95% Wino with a 5% Higgsino component, and the LSP a pure Bino.[12]

Since the two leptons originate from different charginos their flavors are not correlated, and flavor mixing has no effect on this search. However, a smuon-selectron mass difference can actually *improve* the reach for the light slepton in this case. The reason, again, is related to the fact that the analysis [1] utilizes information from the different lepton channels: e^+e^-, $e^\pm\mu^\mp$, etc. With six degenerate sleptons, a chargino decays to either a charged slepton or a sneutrino with equal probability, so the branching fraction for chargino decay to an electron (plus invisible particles) is 1/3. If however, the smuon and the muon-sneutrino are much heavier, this branching fraction goes up to 1/2. In figures 13(a) and 13(b), we compare the limits on the flavor blind models, to the limits on the same models with the smuon decoupled at 600 GeV. Indeed, the reach for the chargino mass is increased by about 100 GeV, while the sensitivity to the LSP mass increases roughly from 150 GeV to 200 GeV. While we chose a large smuon mass for simplicity, even a much smaller mass difference between the selectron and smuon would have an effect.

5.4.2 Limits from $\widetilde{\chi}^\pm\widetilde{\chi}^0_2$ production

The most sensitive searches in this class of models are based on chargino-neutralino production, with $\widetilde{\chi}^+\widetilde{\chi}^0$ ($\widetilde{\chi}^-\widetilde{\chi}^0$) resulting in three leptons $\ell^+\ell^-\ell^+$ ($\ell^+\ell^-\ell^-$), and missing energy. Here, as usual, $\ell = e, \mu$. Note that one OS lepton pair originates from the neutralino decay,

[12] Note that the only difference between the $\widetilde{\ell}_L\widetilde{B}\widetilde{W}$ models considered here and the simplified models considered in [1], is the small Higgsino component in the heavier neutralino and charginos. This has little effect however for left handed sleptons, and particularly for the smuon and selectron.

JHEP10(2015)043

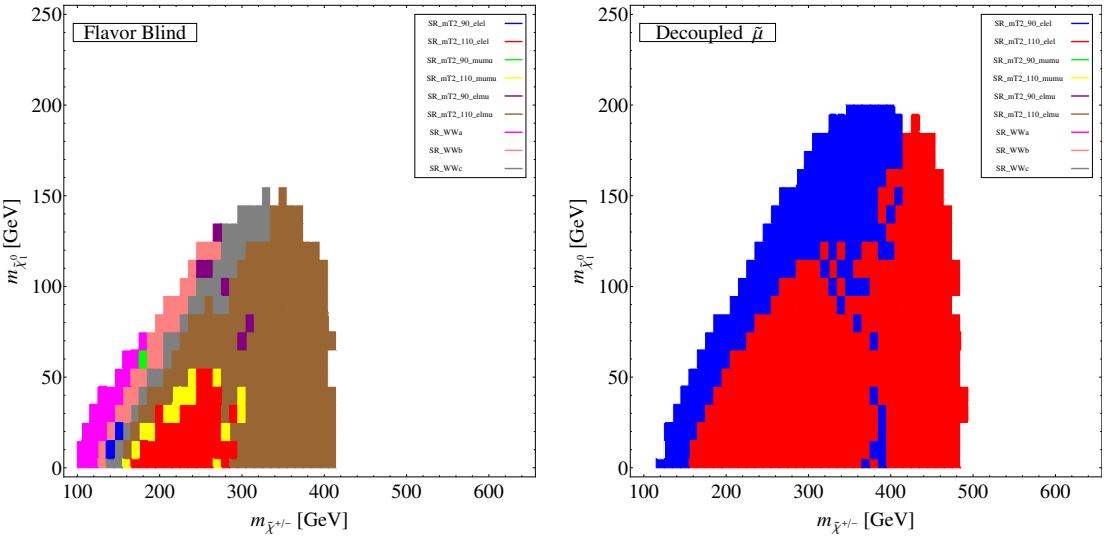

(a) Flavor blind: $\Delta m = 0$, no mixing.

(b) $\tilde{\mu}, \tilde{\nu}_\mu$ decoupled at 600 GeV, no mixing.

Figure 13. The excluded region in the chargino-LSP mass plane, obtained by reinterpreting the search for chargino pair production [1] with subsequesnt decays to OS dileptons plus missing energy for different flavor assumptions: (a) six degenerate L-sleptons halfway between the chargino and LSP masses, with no flavor mixing; (b) same as in (a) but with the smuon and muon-sneutrino decoupled at 600 GeV. The color-coding is as in figure 11.

with the third lepton coming from the chargino. These signatures were used in [77],[13] and interpreted in the context of the $\widetilde{\ell}_L \widetilde{B}\widetilde{W}$ models. Since the slepton spectrum was assumed to be flavor blind, the neutralino decay leads to OSSF leptons. We reproduce the results for this scenario in figure 14(a). Note that the lepton flavor information is not fully utilized in this analysis. Rather, apart from the missing energy, the main requirement is OSSF leptons (electrons *or* muons), plus a third electron or muon, with different signal regions corresponding to the invariant mass of the OSSF pair. As can be seen in figure 14(a), the highest sensitivity is obtained from the SRnoZa, SRnoZb, SRnoZc channels, in which this invariant mass is required to be far from the Z mass. Specifically, $m_{ll} < 60\,\text{GeV}$ in SRnoZa, $60 < m_{ll} < 81.2\,\text{GeV}$ in SRnoZb, and $m_{ll} < 81.2\,\text{GeV}$ or $m_{ll} > 101.2\,\text{GeV}$ in SRnoZc. Similarly, other channels (SRZa, SRZb, SRzc) require this invariant mass to be close to the Z mass in order to increase sensitivity to chargino or neutralino decays into Z bosons.

We now turn to consider models with flavor dependent sleptons. Since the search is essentially a counting experiment, targeting three leptons with charges summing to one, we expect smuon-selectron mixing to have little effect on the results, as long as the sleptons are nearly degenerate. Each slepton mass eigenstate has a 1/6 branching fraction, independently of the mixing. Furthermore, any mixed selectron-smuon states would result in an opposite-sign lepton pair, with each lepton being either an electron or a muon.

[13] Much stronger bounds were obtained by CMS in [6], as can be seen in figure 4. However, such an analysis has been not embedded yet in CheckMATE.

JHEP10(2015)043

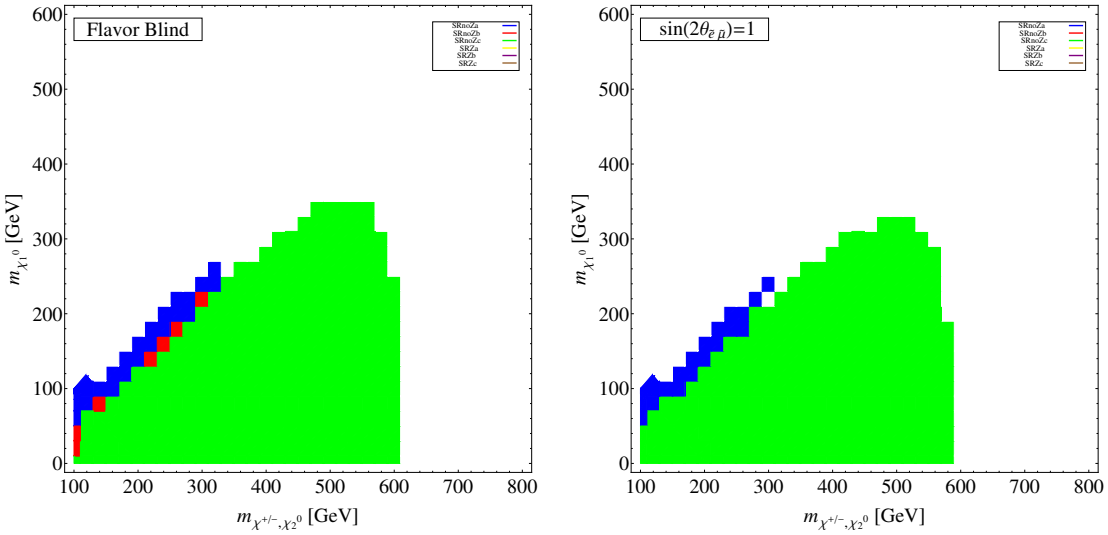

(a) Flavor blind: $\Delta m = 0$, no mixing.

(b) Mixed: small Δm, $\sin 2\theta_{e\mu} = 1$.

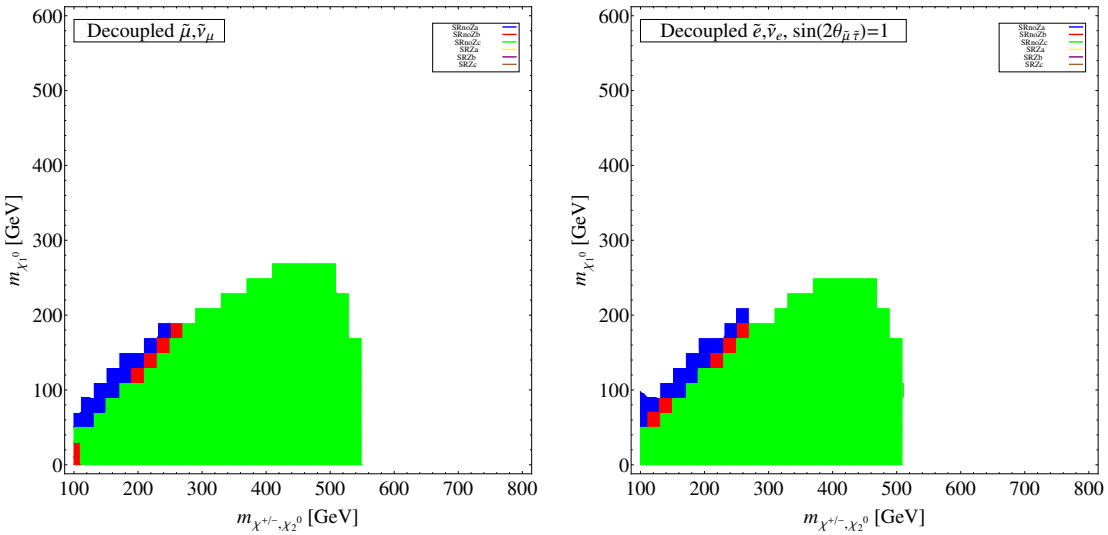

(c) Decoupled $\tilde{\mu}, \tilde{\nu}_\mu$, no mixing.

(d) Decoupled $\tilde{e}, \tilde{\nu}_e$, $\sin 2\theta_{\tilde{\mu}\tilde{\tau}} = 1$.

Figure 14. The excluded region in the chargino-LSP mass plane for $\widetilde{\ell}_L \widetilde{B}\widetilde{W}$ models obtained by reproducing the ATLAS search for $\ell^+\ell^-\ell^\pm$ with one OSSF pair and missing energy from chargino-neutralino pair production, with different assumptions about flavor: (a) flavor blind sleptons halfway between the chargino and LSP masses; (b) same as in (a) but with the selectron and smuon maximally mixed; (c) same as in (a) but with the smuon and smuon sneutrino decoupled at 1 TeV; (d) same as in (a) but with the selectron and electron sneutrino decoupled at 1 TeV, and with maximal smuon-stau mixing.

However, a small fraction of the events would have no OSSF pair, and would therefore not contribute to the ATLAS signal regions, leading to a mild reduction in the sensitivity of the search. This is clearly seen in figure 14(b), where we show the limit for nearly degenerate, maximally mixed selectron-smuon states. The situation would be different in

JHEP10(2015)043

searches looking for kinematic features, such as the kinematic edge associated with the dileptons coming from the neutralino decay. In this case, the $\ell^+\ell^-$ flavor is correlated, and flavor mixing has an important effect [78].

A large mass splitting between the selectron and smuon would have a much larger effect on the analysis. If for example, the smuon and its sneutrino are much heavier than the remaining sleptons, the branching fraction into taus increases at the expense of electrons and muons. The reduced reach is clearly seen in figure 14(c), where the smuon and muon sneutrino are decoupled at 1 TeV. Note that, if lepton flavor information were kept, with electrons and muons treated separately, purely electron trileptons would still be sensitive to the presence of the selectron and the electron sneutrino, which have a larger branching fraction in this case compared to scenarios with three active flavors.

Finally, we consider smuon-stau mixing. Clearly, smuon-stau mixing, or stau-selectron mixing, reduces the sensitivity of these searches. However, as long as the slepton states are close in mass, the number of $\ell^\pm\ell^\mp\ell^+$ (or $\ell^\pm\ell^\mp\ell^-$) trileptons remains essentially the same. In figure 14(d), we modify the model by taking the selectron (and its sneutrino) to be very heavy, with, in addition, maximally-mixed smuon-stau states halfway between the LSP and the heavy gauginos. Indeed, the reach is significantly lower in this case. Note that this scenario, under the hypothesis of no mixing involving the selectron, is only constrained by $\tau \to \mu\gamma$, but as can be seen in figure 4, this gives no constraint on the flavor parameters at present. For completeness, in figure 15(a), we show the bounds from $\mu \to e\gamma$ (dark hatched region) together with the LHC results. The excluded region for the flavor blind model is also shown (dark grey) for reference. Similarly, figure 15(b) displays the limits on models with decoupled selectrons and with smuon-stau mixing, compared to the flavor-blind models. All of the parameter space is compatible with $\tau \to \mu\gamma$ in this case.

6 Conclusions

Low energy constraints on slepton flavor are often interpreted in terms of minimal supersymmetric extensions of the standard model, with all superpartner masses determined by a few parameters. If there is anything the first LHC run has taught us however, both through direct searches and through the measurement of the Higgs mass, is that we should be wary of minimal theoretical frameworks when searching for supersymmetry. With this in mind, we adopted a model independent approach to analyze the implications of low energy bounds on flavor dependent spectra, and the LHC signatures of viable models.

Since we are interested in scenarios with both small and large slepton mass differences, we computed the low-energy flavor-violating (as well as flavor-conserving) dipole amplitudes in the mass-eigenstate basis. We obtained compact expressions for the amplitudes, classified according to the the ways in which the chirality flip is implemented.

Then, with the aim of comparing the sensitivity of CLFV and LHC experiments to flavor dependent slepton spectra, we systematically classified the simplified models involving only non-colored superpartners, with at most three different mass scales. Some of these models were employed by the LHC collaborations to interpret their searches for electroweak production of sleptons, neutralinos and charginos. The quantity constrained by CLFV is

JHEP10(2015)043

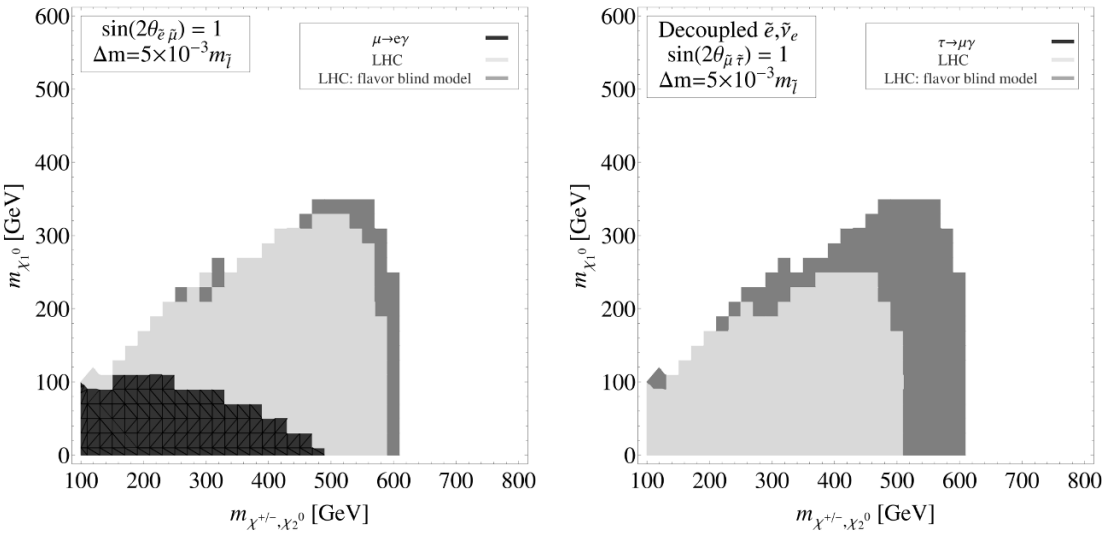

(a) $\Delta m_{\tilde{e}\tilde{\mu}} = 5 \times 10^{-3} m$, $\sin 2\theta_{\tilde{e}\tilde{\mu}} = 1$.

(b) $\Delta m_{\tilde{\mu}\tilde{\tau}} = 5 \times 10^{-3} m$, $\sin 2\theta_{\tilde{\mu}\tilde{\tau}} = 1$.

Figure 15. The excluded region (light grey) in the chargino-LSP mass plane for $\widetilde{\ell}_L \widetilde{B} \widetilde{W}$ models obtained by reproducing the ATLAS search for $\ell^+\ell^-\ell^\pm$ with one OSSF pair and missing energy from chargino-neutralino pair production, with different assumptions about flavor: (a) maximal selectron-smuon mixing with $\Delta m_{\tilde{e}\tilde{\mu}} = 5 \times 10^{-3} m$; (b) decoupled $\tilde{e}$, $\tilde{\nu}_e$, maximal $\tilde{\mu} - \tilde{\tau}$ mixing with $\Delta m_{\tilde{\mu}\tilde{\tau}} = 5 \times 10^{-3} m$. The dark hatched region is excluded by $\mu \to e\gamma$. The dark grey indicates the excluded region of figure 14(a) (flavor blind sleptons) which is now allowed.

schematically given by,

$$\frac{1}{\widetilde{m}^2}\,\delta \sim \frac{1}{\widetilde{m}^2}\,\frac{\Delta\widetilde{m}}{\widetilde{m}}\,\sin 2\theta\,. \tag{6.1}$$

For each of the simplified models, we derived the CLFV bound on δ for a small mass splitting $\Delta\widetilde{m}$, as a function of the superpartner masses, showing also the current LHC limits on flavor-blind sleptons, and, whenever possible, the projected 14 TeV bounds. As is evident from our plots of section 4, there is an interesting interplay between low-energy and high-energy bounds. In particular, since the cross-sections for superpartner production fall very fast with the superpartner mass, whereas the contributions of heavy superpartners to CLFV processes decouple more slowly, low-energy channels are the best probes of CLFV for heavy spectra. Moreover, LHC bounds are rather loose for compressed spectra, in contrast to CLFV processes.

We then turned to LHC searches. Using our results for the allowed flavor dependence, we considered a few simplified models with either large slepton mass differences or large selectron-smuon or smuon-stau mixing. We reinterpreted several ATLAS analyses to obtain the allowed regions in the parameter space of these models. In some cases, flavor dependence significantly modifies the reach of the searches. Since the next LHC run will probe regions in which larger flavor effects are allowed, it is important that full flavor information is retained in the experimental analyses, and that future searches are interpreted taking into account the possible large flavor mixing in the slepton sector.

JHEP10(2015)043

Acknowledgments

IG thanks David Cohen, the ATLAS-Technion computer grid administrator, for extensive computer assistance. IG also thanks Jamie Tattersall for useful discussions. LC and PP thank the Technion Center for Particle Physics for hospitality and financial support while some of this work was completed. The research of YS was supported by the Israel Science Foundation (ISF) under grant No. 1367/11, by the United States-Israel Binational Science Foundation (BSF) under grant No. 2010221, and by the ICORE Program of the Planning and Budgeting Committee (Grant No. 1937/12). IG is supported by NSF grant PHY-1316792. AM gratefully acknowledges support by the research grant Theoretical Astroparticle Physics No. 2012CPPPYP7 under the program PRIN 2012 funded by the Ministero dell'Istruzione, Università e della Ricerca (MIUR). The research of AM and PP is also supported by the ERC Advanced Grant No. 267985 (DaMeSyFla) and by the research grant TAsP (Theoretical Astroparticle Physics), by the Istituto Nazionale di Fisica Nucleare (INFN).

A Expressions for the leptonic dipoles

We now present the full expressions for the $\ell_i \to \ell_j\gamma$ amplitudes, $(g-2)_\mu$ and d_e distinguishing among the ways in which the chirality flip is implemented. In order to simplify the expressions as much as possible, while retaining the salient flavor features, we treat SU(2) breaking effects in the chargino/neutralino mass-matrices as perturbations [48]. On the other hand, we work in the mass eigenstate basis for the sleptons assuming a two generation scheme.

A.1 $\ell_i \to \ell_j\gamma$

In the following, we give the relevant amplitudes for $\ell_i \to \ell_j\gamma$ both in the mass eigenstate basis and in the MIA. As a first class of contributions, we consider the amplitudes in which the chirality flip is realized on the external fermion line. In this case we have,

$$(A_L^{c_1})_{\mathrm{SU(2)}} = -\frac{\alpha_2}{8\pi}\sin\theta_L\cos\theta_L\left[\frac{f_c^L(x_{2\tilde{\ell}_1})}{m^2_{\tilde{\ell}_1}} - \frac{f_c^L(x_{2\tilde{\ell}_2})}{m^2_{\tilde{\ell}_2}}\right], \tag{A.1}$$

$$(A_L^{n_1})_{\mathrm{SU(2)}} = \frac{\alpha_2}{16\pi}\sin\theta_L\cos\theta_L\left[\frac{f_n^L(x_{2\tilde{\ell}_1})}{m^2_{\tilde{\ell}_1}} - \frac{f_n^L(x_{2\tilde{\ell}_2})}{m^2_{\tilde{\ell}_2}}\right], \tag{A.2}$$

$$(A_L^{n_1})_{\mathrm{U(1)}} = \frac{\alpha_Y}{16\pi}\sin\theta_L\cos\theta_L\left[\frac{f_n^L(x_{1\tilde{\ell}_1})}{m^2_{\tilde{\ell}_1}} - \frac{f_n^L(x_{1\tilde{\ell}_2})}{m^2_{\tilde{\ell}_2}}\right], \tag{A.3}$$

$$(A_R^{n_1})_{\mathrm{U(1)}} = \frac{\alpha_Y}{4\pi}\sin\theta_R\cos\theta_R\left[\frac{f_n^L(x_{1\tilde{e}_1})}{m^2_{\tilde{e}_1}} - \frac{f_n^L(x_{1\tilde{e}_2})}{m^2_{\tilde{e}_2}}\right], \tag{A.4}$$

where we have defined the ratios $x_{I\tilde{\ell}_j} = |M_I^2|/m^2_{\tilde{\ell}_j}$, where M_1 (M_2) is the Bino (Wino) mass parameter, $x_{I\tilde{e}_j} = |M_I^2|/m^2_{\tilde{e}_j}$, $x_{\mu\tilde{\ell}_j} = |\mu|^2/m^2_{\tilde{\ell}_j}$, and $x_{\mu\tilde{e}_j} = |\mu|^2/m^2_{\tilde{e}_j}$.

JHEP10(2015)043

The corresponding MIA expressions read

$$(A_L^{c_1})^{\rm MIA}_{\rm SU(2)} = \frac{\alpha_2}{4\pi}\frac{\Delta^{21}_{LL}}{m_L^4} f_{1c}(x_{2L})\,, \tag{A.5}$$

$$(A_L^{n_1})^{\rm MIA}_{\rm SU(2)} = \frac{\alpha_2}{4\pi}\frac{\Delta^{21}_{LL}}{m_L^4} f_{1n}(x_{2L})\,, \tag{A.6}$$

$$(A_L^{n_1})^{\rm MIA}_{\rm U(1)} = \frac{\alpha_Y}{4\pi}\frac{\Delta^{21}_{LL}}{m_L^4} f_{1n}(x_{1L})\,, \tag{A.7}$$

$$(A_R^{n_1})^{\rm MIA}_{\rm U(1)} = \frac{\alpha_Y}{\pi}\frac{\Delta^{21}_{RR}}{m_R^4} f_{1n}(x_{1R})\,. \tag{A.8}$$

If the chirality flip occurs on the Yukawa vertex, we have the following amplitudes,

$$(A_L^{c_2})_{\rm SU(2)} = \frac{\alpha_2}{8\pi}\sin\theta_L\cos\theta_L\left[a_2\,\frac{f_c^{LR}(x_{2\widetilde{\ell}_1})}{m^2_{\widetilde{\ell}_1}} - b_2\,\frac{f_c^{LR}(x_{\mu\widetilde{\ell}_1})}{m^2_{\widetilde{\ell}_1}} - (\widetilde{\ell}_1\leftrightarrow\widetilde{\ell}_2)\right], \tag{A.9}$$

$$(A_L^{n_2})_{\rm SU(2)} = -\frac{\alpha_2}{8\pi}\sin\theta_L\cos\theta_L\left[a_2\,\frac{f_{3n}(x_{2\widetilde{\ell}_1})}{m^2_{\widetilde{\ell}_1}} - b_2\,\frac{f_{3n}(x_{\mu\widetilde{\ell}_1})}{m^2_{\widetilde{\ell}_1}} - (\widetilde{\ell}_1\leftrightarrow\widetilde{\ell}_2)\right], \tag{A.10}$$

$$(A_L^{n_2})_{\rm U(1)} = \frac{\alpha_Y}{8\pi}\sin\theta_L\cos\theta_L\left[a_1\,\frac{f_{3n}(x_{1\widetilde{\ell}_1})}{m^2_{\widetilde{\ell}_1}} - b_1\,\frac{f_{3n}(x_{\mu\widetilde{\ell}_1})}{m^2_{\widetilde{\ell}_1}} - (\widetilde{\ell}_1\leftrightarrow\widetilde{\ell}_2)\right], \tag{A.11}$$

$$(A_R^{n_2})_{\rm U(1)} = -\frac{\alpha_Y}{4\pi}\sin\theta_R\cos\theta_R\left[a_1\,\frac{f_{3n}(x_{1\widetilde{e}_1})}{m^2_{\widetilde{e}_1}} - b_1\,\frac{f_{3n}(x_{\mu\widetilde{e}_1})}{m^2_{\widetilde{e}_1}} - (\widetilde{e}_1\leftrightarrow\widetilde{e}_2)\right], \tag{A.12}$$

where we have defined the quantities

$$a_1 = \frac{(|M_1|^2+\mu M_1 t_\beta)}{|M_1|^2-|\mu|^2}\,, \qquad a_2 = \frac{(|M_2|^2+\mu M_2 t_\beta)}{|M_2|^2-|\mu|^2}\,, \tag{A.13}$$

$$b_1 = \frac{(|\mu|^2+\mu M_1 t_\beta)}{|M_1|^2-|\mu|^2}\,, \qquad b_2 = \frac{(|\mu|^2+\mu M_2 t_\beta)}{|M_2|^2-|\mu|^2}\,. \tag{A.14}$$

The corresponding MIA amplitudes are

$$(A_L^{c_2})^{\rm MIA}_{\rm SU(2)} = \frac{\alpha_2}{4\pi}\frac{\Delta^{21}_{LL}}{m_L^4}\left[a_2 f_{2c}(x_{2L}) - b_2 f_{2c}(x_{\mu L})\right], \tag{A.15}$$

$$(A_L^{n_2})^{\rm MIA}_{\rm SU(2)} = \frac{\alpha_2}{4\pi}\frac{\Delta^{21}_{LL}}{m_L^4}\left[a_2 f_{2n}(x_{2L}) - b_2 f_{2n}(x_{\mu L})\right], \tag{A.16}$$

$$(A_L^{n_2})^{\rm MIA}_{\rm U(1)} = -\frac{\alpha_Y}{4\pi}\frac{\Delta^{21}_{LL}}{m_L^4}\left[a_1 f_{2n}(x_{1L}) - b_1 f_{2n}(x_{\mu L})\right], \tag{A.17}$$

$$(A_R^{n_2})^{\rm MIA}_{\rm U(1)} = \frac{\alpha_Y}{2\pi}\frac{\Delta^{21}_{RR}}{m_R^4}\left[a_1 f_{2n}(x_{1R}) - b_1 f_{2n}(x_{\mu R})\right]. \tag{A.18}$$

Finally, the amplitudes corresponding to a chirality flip on the internal sfermion line read

$$\begin{aligned}(A_L^{n_3})_{\rm U(1)} = &-\frac{\alpha_Y}{4\pi}\frac{M_1}{m_\mu}\Delta^{22}_{RL}\sin\theta_L\cos\theta_L\left[\left(\frac{f_{3n}(x_{1R})}{m^2_{R_2}} - \frac{f_{3n}(x_{1\widetilde{\ell}_1})}{m^2_{\widetilde{\ell}_1}}\right)\frac{1}{(m^2_{R_2}-m^2_{\widetilde{\ell}_1})} - (\widetilde{\ell}_1\leftrightarrow\widetilde{\ell}_2)\right]\\ &-\frac{\alpha_Y}{4\pi}\frac{M_1}{m_\mu}\frac{\Delta^{21}_{RL}}{m^2_{\widetilde{\ell}_1}-m^2_{R_2}}\left[\frac{f_{3n}(x_{1\widetilde{\ell}_1})}{m^2_{\widetilde{\ell}_1}} - \frac{f_{3n}(x_{1R})}{m^2_{R_2}}\right],\end{aligned} \tag{A.19}$$

JHEP10(2015)043

$$(A_R^{n_3})_{\mathrm{U}(1)} = -\frac{\alpha_Y}{4\pi}\frac{M_1}{m_\mu}\Delta_{LR}^{22}\sin\theta_R\cos\theta_R\left[\left(\frac{f_{3n}(x_{1L})}{m_{L_2}^2}-\frac{f_{3n}(x_{1\widetilde{e}_1})}{m_{\widetilde{e}_1}^2}\right)\frac{1}{(m_{L_2}^2-m_{\widetilde{e}_1}^2)}-(\widetilde{e}_1\leftrightarrow\widetilde{e}_2)\right]$$
$$-\frac{\alpha_Y}{4\pi}\frac{M_1}{m_\mu}\frac{\Delta_{LR}^{21}}{m_{\widetilde{e}_1}^2-m_{L_2}^2}\left[\frac{f_{3n}(x_{1\widetilde{e}_1})}{m_{\widetilde{e}_1}^2}-\frac{f_{3n}(x_{1L})}{m_{L_2}^2}\right], \tag{A.20}$$

where $\Delta_{RL}^{22} = m_\mu(A_\mu - \mu^* t_\beta)$.

The MIA expressions for this last case are the following

$$(A_L^{n_3})_{\mathrm{U}(1)}^{\mathrm{MIA}} = \frac{\alpha_Y}{4\pi}\frac{M_1}{m_\mu}\frac{\Delta_{RL}^{22}\Delta_{LL}^{21}}{(m_L^2-m_R^2)}\left[\frac{2f_{2n}(x_{1L})}{m_L^4}+\frac{1}{m_L^2-m_R^2}\left(\frac{f_{3n}(x_{1L})}{m_L^2}-\frac{f_{3n}(x_{1R})}{m_R^2}\right)\right]$$
$$-\frac{\alpha_Y}{4\pi}\frac{M_1}{m_\mu}\frac{\Delta_{RL}^{21}}{m_L^2-m_R^2}\left[\frac{f_{3n}(x_{1L})}{m_L^2}-\frac{f_{3n}(x_{1R})}{m_R^2}\right], \tag{A.21}$$

$$(A_R^{n_3})_{\mathrm{U}(1)}^{\mathrm{MIA}} = \frac{\alpha_Y}{4\pi}\frac{M_1}{m_\mu}\frac{\Delta_{LR}^{22}\Delta_{RR}^{21}}{(m_R^2-m_L^2)}\left[\frac{2f_{2n}(x_{1R})}{m_R^4}+\frac{1}{m_R^2-m_L^2}\left(\frac{f_{3n}(x_{1R})}{m_R^2}-\frac{f_{3n}(x_{1L})}{m_L^2}\right)\right]$$
$$-\frac{\alpha_Y}{4\pi}\frac{M_1}{m_\mu}\frac{\Delta_{LR}^{21}}{m_R^2-m_L^2}\left[\frac{f_{3n}(x_{1R})}{m_R^2}-\frac{f_{3n}(x_{1L})}{m_L^2}\right]. \tag{A.22}$$

A.2 $(g-2)_\mu$

The supersymmetric effects for $\Delta a_\mu = (g-2)_\mu/2$ are such that $\Delta a_\mu = \Delta a_\mu^{(n)} + \Delta a_\mu^{(c)}$ where $\Delta a_\mu^{(n)}$ and $\Delta a_\mu^{(c)}$ arise from the neutralino and chargino contributions, respectively. The contributions where the chirality flip is realized on the external fermion line read

$$\left(\Delta a_\mu^{n_1}\right)_{\mathrm{U}(1)}^R = -\frac{\alpha_Y}{2\pi}\frac{m_\mu^2}{m_R^2}\,f_n^L(x_{1R}), \tag{A.23}$$

$$\left(\Delta a_\mu^{n_1}\right)_{\mathrm{U}(1)}^L = -\frac{\alpha_Y}{8\pi}\frac{m_\mu^2}{m_L^2}\,f_n^L(x_{1L}), \tag{A.24}$$

$$\left(\Delta a_\mu^{n_1}\right)_{\mathrm{SU}(2)} = -\frac{\alpha_2}{8\pi}\frac{m_\mu^2}{m_L^2}f_n^L(x_{2L}), \tag{A.25}$$

$$\left(\Delta a_\mu^{c_1}\right)_{\mathrm{SU}(2)} = \frac{\alpha_2}{4\pi}\frac{m_\mu^2}{m_L^2}f_c^L(x_{2L}), \tag{A.26}$$

while, in the case where the chirality flip is realized at the Yukawa vertex, we find

$$\left(\Delta a_\mu^{n_2}\right)_{\mathrm{U}(1)}^R = \frac{\alpha_Y}{2\pi}\frac{m_\mu^2}{m_R^2}\left[\mathrm{Re}(a_1)f_{3n}(x_{1R}) - \mathrm{Re}(b_1)f_{3n}(x_{\mu R})\right], \tag{A.27}$$

$$\left(\Delta a_\mu^{n_2}\right)_{\mathrm{U}(1)}^L = -\frac{\alpha_Y}{4\pi}\frac{m_\mu^2}{m_L^2}\left[\mathrm{Re}(a_1)f_{3n}(x_{1L}) - \mathrm{Re}(b_1)f_{3n}(x_{\mu L})\right], \tag{A.28}$$

$$\left(\Delta a_\mu^{n_2}\right)_{\mathrm{SU}(2)} = \frac{\alpha_2}{4\pi}\frac{m_\mu^2}{m_L^2}\left[\mathrm{Re}(a_2)f_{3n}(x_{2L}) - \mathrm{Re}(b_2)f_{3n}(x_{\mu L})\right], \tag{A.29}$$

$$\left(\Delta a_\mu^{c_2}\right)_{\mathrm{SU}(2)} = -\frac{\alpha_2}{4\pi}\frac{m_\mu^2}{m_L^2}\left[\mathrm{Re}(a_2)f_c^{LR}(x_{2L}) - \mathrm{Re}(b_2)f_c^{LR}(x_{\mu L})\right]. \tag{A.30}$$

Finally, the amplitude relative to a chirality flip at the internal sfermion line is given by

$$\left(\Delta a_\mu^{n_3}\right)_{\mathrm{U}(1)} = \frac{\alpha_Y}{2\pi}\frac{m_\mu}{m_L^2-m_R^2}\mathrm{Re}(M_1 m_{LR}^2)_{22}\left[\frac{f_{3n}(x_{1L})}{m_L^2}-\frac{f_{3n}(x_{1R})}{m_R^2}\right]. \tag{A.31}$$

JHEP10(2015)043

A.3 Electron EDM

The supersymmetric effects for the electron EDM d_e are given by $d_e = d_e^{(n)} + d_e^{(c)}$ where $d_e^{(n)}$ and $d_e^{(c)}$ arise from the neutralino and chargino contributions, respectively. In contrast to the $g-2$ and $\mu \to e\gamma$ contributions, d_e does not receive contributions from a chirality flip implemented on the external fermion line, as the resulting amplitude is real. The amplitudes arising from a chirality flip at the Yukawa vertex read

$$\left(\frac{d_e^{n_2}}{e}\right)^R_{\mathrm{U}(1)} = \frac{\alpha_Y}{4\pi}\frac{m_e}{m_R^2}\frac{\mathrm{Im}(\mu M_1)}{M_1^2-\mu^2} t_\beta \left[f_{3n}(x_{1R}) - f_{3n}(x_{\mu R})\right] , \tag{A.32}$$

$$\left(\frac{d_e^{n_2}}{e}\right)^L_{\mathrm{U}(1)} = -\frac{\alpha_Y}{8\pi}\frac{m_e}{m_L^2}\frac{\mathrm{Im}(\mu M_1)}{M_1^2-\mu^2} t_\beta \left[f_{3n}(x_{1L}) - f_{3n}(x_{\mu L})\right] , \tag{A.33}$$

$$\left(\frac{d_e^{n_2}}{e}\right)_{\mathrm{SU}(2)} = \frac{\alpha_2}{8\pi}\frac{m_e}{m_L^2}\frac{\mathrm{Im}(\mu M_2)}{M_2^2-\mu^2} t_\beta \left[f_{3n}(x_{2L}) - f_{3n}(x_{\mu L})\right] , \tag{A.34}$$

$$\left(\frac{d_e^{c_2}}{e}\right)_{\mathrm{SU}(2)} = -\frac{\alpha_2}{8\pi}\frac{m_e}{m_L^2}\frac{\mathrm{Im}(\mu M_2)}{M_2^2-\mu^2} t_\beta \left[f_c^{LR}(x_{2L}) - f_c^{LR}(x_{\mu L})\right] , \tag{A.35}$$

while those from a chirality flip at the internal sfermion line are given by

$$\left(\frac{d_e^{n_3}}{e}\right)_{\mathrm{U}(1)} = \frac{\alpha_Y}{4\pi}\frac{\mathrm{Im}(M_1 m_{LR}^2)_{11}}{m_L^2-m_R^2}\left[\frac{f_{3n}(x_{1L})}{m_L^2} - \frac{f_{3n}(x_{1R})}{m_R^2}\right] . \tag{A.36}$$

A.4 Loop functions

In this appendix we report the explicit expressions for the loop functions:

$$f_{1n}(x) = \frac{-17x^3+9x^2+9x-1+6x^2(x+3)\ln x}{24(1-x)^5} , \tag{A.37}$$

$$f_{2n}(x) = \frac{-5x^2+4x+1+2x(x+2)\ln x}{4(1-x)^4} , \tag{A.38}$$

$$f_{3n}(x) = \frac{1+2x\ln x - x^2}{2(1-x)^3} , \tag{A.39}$$

$$f_{1c}(x) = \frac{-x^3-9x^2+9x+1+6x(x+1)\ln x}{6(1-x)^5} , \tag{A.40}$$

$$f_{2c}(x) = \frac{-x^2-4x+5+2(2x+1)\ln x}{2(1-x)^4} , \tag{A.41}$$

$$f_n^L(x) = \frac{1-6x+3x^2+2x^3-6x^2\log x}{6(1-x)^4} , \tag{A.42}$$

$$f_c^L(x) = \frac{2+3x-6x^2+x^3+6x\log x}{6(1-x)^4} , \tag{A.43}$$

$$f_c^{LR}(x) = \frac{-3+4x-x^2-2\log x}{(1-x)^3} . \tag{A.44}$$

JHEP10(2015)043

References

[1] ATLAS collaboration, *Search for direct-slepton and direct-chargino production in final states with two opposite-sign leptons, missing transverse momentum and no jets in 20/fb of pp collisions at $\sqrt{s} = 8$ TeV with the ATLAS detector*, ATLAS-CONF-2013-049 (2013).

[2] CMS collaboration, *Search for electroweak production of charginos, neutralinos and sleptons using leptonic final states in pp collisions at 8 TeV*, CMS-PAS-SUS-13-006 (2013).

[3] ATLAS collaboration, *Search for direct production of charginos and neutralinos in events with three leptons and missing transverse momentum in $\sqrt{s} = 8$ TeV pp collisions with the ATLAS detector*, *JHEP* **04** (2014) 169 [arXiv:1402.7029] [INSPIRE].

[4] ATLAS collaboration, *Search for direct production of charginos, neutralinos and sleptons in final states with two leptons and missing transverse momentum in pp collisions at $\sqrt{s} = 8$ TeV with the ATLAS detector*, *JHEP* **05** (2014) 071 [arXiv:1403.5294] [INSPIRE].

[5] ATLAS collaboration, *Search for supersymmetry in events with four or more leptons in $\sqrt{s} = 8$ TeV pp collisions with the ATLAS detector*, *Phys. Rev.* **D 90** (2014) 052001 [arXiv:1405.5086] [INSPIRE].

[6] CMS collaboration, *Searches for electroweak production of charginos, neutralinos and sleptons decaying to leptons and W, Z and Higgs bosons in pp collisions at 8 TeV*, *Eur. Phys. J.* **C 74** (2014) 3036 [arXiv:1405.7570] [INSPIRE].

[7] MUON G-2 collaboration, G.W. Bennett et al., *Final Report of the Muon E821 Anomalous Magnetic Moment Measurement at BNL*, *Phys. Rev.* **D 73** (2006) 072003 [hep-ex/0602035] [INSPIRE].

[8] F. Jegerlehner and A. Nyffeler, *The Muon g-2*, *Phys. Rept.* **477** (2009) 1 [arXiv:0902.3360] [INSPIRE].

[9] K. Hagiwara, R. Liao, A.D. Martin, D. Nomura and T. Teubner, *$(g-2)_\mu$ and $\alpha(M_Z^2)$ re-evaluated using new precise data*, *J. Phys.* **G 38** (2011) 085003 [arXiv:1105.3149] [INSPIRE].

[10] M. Davier, A. Hoecker, B. Malaescu and Z. Zhang, *Reevaluation of the Hadronic Contributions to the Muon g-2 and to $\alpha(M_Z^2)$*, *Eur. Phys. J.* **C 71** (2011) 1515 [*Erratum ibid.* **C 72** (2012) 1874] [arXiv:1010.4180] [INSPIRE].

[11] BESIII collaboration, A. Denig, *Measurements of the Hadronic Cross section and of Meson Transition Form Factors at BESIII for an improved Standard Model Prediction of $(g-2)_\mu$*, *Nucl. Part. Phys. Proc.* **260** (2015) 79 [arXiv:1412.2951] [INSPIRE].

[12] J.L. Feng, K.T. Matchev and Y. Shadmi, *Theoretical expectations for the muon's electric dipole moment*, *Nucl. Phys.* **B 613** (2001) 366 [hep-ph/0107182] [INSPIRE].

[13] G.F. Giudice, P. Paradisi and M. Passera, *Testing new physics with the electron g-2*, *JHEP* **11** (2012) 113 [arXiv:1208.6583] [INSPIRE].

JHEP10(2015)043

[14] J.L. Feng, C.G. Lester, Y. Nir and Y. Shadmi, *The Standard Model and Supersymmetric Flavor Puzzles at the Large Hadron Collider*, *Phys. Rev.* **D 77** (2008) 076002 [arXiv:0712.0674] [INSPIRE].

[15] G.D. Kribs, E. Poppitz and N. Weiner, *Flavor in supersymmetry with an extended R-symmetry*, *Phys. Rev.* **D 78** (2008) 055010 [arXiv:0712.2039] [INSPIRE].

[16] Y. Nomura, M. Papucci and D. Stolarski, *Flavorful Supersymmetry from Higher Dimensions*, *JHEP* **07** (2008) 055 [arXiv:0802.2582] [INSPIRE].

[17] Y. Nomura and D. Stolarski, *Naturally Flavorful Supersymmetry at the LHC*, *Phys. Rev.* **D 78** (2008) 095011 [arXiv:0808.1380] [INSPIRE].

[18] Y. Shadmi and P.Z. Szabo, *Flavored Gauge-Mediation*, *JHEP* **06** (2012) 124 [arXiv:1103.0292] [INSPIRE].

[19] N. Craig, M. McCullough and J. Thaler, *The New Flavor of Higgsed Gauge Mediation*, *JHEP* **03** (2012) 049 [arXiv:1201.2179] [INSPIRE].

[20] L. Calibbi, Z. Lalak, S. Pokorski and R. Ziegler, *The Messenger Sector of SUSY Flavour Models and Radiative Breaking of Flavour Universality*, *JHEP* **06** (2012) 018 [arXiv:1203.1489] [INSPIRE].

[21] N. Craig, M. McCullough and J. Thaler, *Flavor Mediation Delivers Natural SUSY*, *JHEP* **06** (2012) 046 [arXiv:1203.1622] [INSPIRE].

[22] L. Calibbi, P. Paradisi and R. Ziegler, *Lepton Flavor Violation in Flavored Gauge Mediation*, *Eur. Phys. J.* **C 74** (2014) 3211 [arXiv:1408.0754] [INSPIRE].

[23] Y. Nir and N. Seiberg, *Should squarks be degenerate?*, *Phys. Lett.* **B 309** (1993) 337 [hep-ph/9304307] [INSPIRE].

[24] M. Abdullah, I. Galon, Y. Shadmi and Y. Shirman, *Flavored Gauge Mediation, A Heavy Higgs and Supersymmetric Alignment*, *JHEP* **06** (2013) 057 [arXiv:1209.4904] [INSPIRE].

[25] I. Galon, G. Perez and Y. Shadmi, *Non-Degenerate Squarks from Flavored Gauge Mediation*, *JHEP* **09** (2013) 117 [arXiv:1306.6631] [INSPIRE].

[26] L. Calibbi, A. Mariotti, C. Petersson and D. Redigolo, *Selectron NLSP in Gauge Mediation*, *JHEP* **09** (2014) 133 [arXiv:1405.4859] [INSPIRE].

[27] J. Hisano, M. Nagai and P. Paradisi, *Electric dipole moments from flavor-changing supersymmetric soft terms*, *Phys. Rev.* **D 78** (2008) 075019 [arXiv:0712.1285] [INSPIRE].

[28] J. Hisano, M. Nagai and P. Paradisi, *Flavor effects on the electric dipole moments in supersymmetric theories: A beyond leading order analysis*, *Phys. Rev.* **D 80** (2009) 095014 [arXiv:0812.4283] [INSPIRE].

[29] G. Raz, *The mass insertion approximation without squark degeneracy*, *Phys. Rev.* **D 66** (2002) 037701 [hep-ph/0205310] [INSPIRE].

[30] Y. Nir and G. Raz, *Quark squark alignment revisited*, *Phys. Rev.* **D 66** (2002) 035007 [hep-ph/0206064] [INSPIRE].

[31] MEG collaboration, J. Adam et al., *New constraint on the existence of the $\mu^+ \to e^+\gamma$ decay*, *Phys. Rev. Lett.* **110** (2013) 201801 [arXiv:1303.0754] [INSPIRE].

[32] A.M. Baldini et al., *MEG Upgrade Proposal*, arXiv:1301.7225 [INSPIRE].

JHEP10(2015)043

[33] SINDRUM collaboration, U. Bellgardt et al., *Search for the Decay $\mu^+ \to e^+e^+e^-$*, *Nucl. Phys.* **B 299** (1988) 1 [INSPIRE].

[34] A. Blondel et al., *Research Proposal for an Experiment to Search for the Decay $\mu \to eee$*, arXiv:1301.6113 [INSPIRE].

[35] SINDRUM II collaboration, W.H. Bertl et al., *A search for muon to electron conversion in muonic gold*, *Eur. Phys. J.* **C 47** (2006) 337 [INSPIRE].

[36] SINDRUM II collaboration, C. Dohmen et al., *Test of lepton flavor conservation in $\mu \to e$ conversion on titanium*, *Phys. Lett.* **B 317** (1993) 631 [INSPIRE].

[37] COMET collaboration, http://comet.kek.jp/Documents.html.

[38] MU2E collaboration, R.J. Abrams et al., *Mu2e Conceptual Design Report*, arXiv:1211.7019 [INSPIRE].

[39] BABAR collaboration, B. Aubert et al., *Searches for Lepton Flavor Violation in the Decays $\tau^\pm \to e^\pm\gamma$ and $\tau^\pm \to \mu^\pm\gamma$*, *Phys. Rev. Lett.* **104** (2010) 021802 [arXiv:0908.2381] [INSPIRE].

[40] BELLE, BELLE-II collaboration, K. Hayasaka, *Results and prospects on lepton flavor violation at Belle/Belle II*, *J. Phys. Conf. Ser.* **408** (2013) 012069 [INSPIRE].

[41] K. Hayasaka et al., *Search for Lepton Flavor Violating τ Decays into Three Leptons with 719 Million Produced $\tau^+\tau^-$ Pairs*, *Phys. Lett.* **B 687** (2010) 139 [arXiv:1001.3221] [INSPIRE].

[42] ACME collaboration, J. Baron et al., *Order of Magnitude Smaller Limit on the Electric Dipole Moment of the Electron*, *Science* **343** (2014) 269 [arXiv:1310.7534] [INSPIRE].

[43] F. Borzumati and A. Masiero, *Large Muon and electron Number Violations in Supergravity Theories*, *Phys. Rev. Lett.* **57** (1986) 961 [INSPIRE].

[44] J. Hisano, T. Moroi, K. Tobe and M. Yamaguchi, *Lepton flavor violation via right-handed neutrino Yukawa couplings in supersymmetric standard model*, *Phys. Rev.* **D 53** (1996) 2442 [hep-ph/9510309] [INSPIRE].

[45] F. Gabbiani and A. Masiero, *FCNC in Generalized Supersymmetric Theories*, *Nucl. Phys.* **B 322** (1989) 235 [INSPIRE].

[46] F. Gabbiani, E. Gabrielli, A. Masiero and L. Silvestrini, *A complete analysis of FCNC and CP constraints in general SUSY extensions of the standard model*, *Nucl. Phys.* **B 477** (1996) 321 [hep-ph/9604387] [INSPIRE].

[47] I. Masina and C.A. Savoy, *Sleptonarium: Constraints on the CP and flavor pattern of scalar lepton masses*, *Nucl. Phys.* **B 661** (2003) 365 [hep-ph/0211283] [INSPIRE].

[48] P. Paradisi, *Constraints on SUSY lepton flavor violation by rare processes*, *JHEP* **10** (2005) 006 [hep-ph/0505046] [INSPIRE].

[49] E. Arganda and M.J. Herrero, *Testing supersymmetry with lepton flavor violating tau and mu decays*, *Phys. Rev.* **D 73** (2006) 055003 [hep-ph/0510405] [INSPIRE].

[50] M. Arana-Catania, S. Heinemeyer and M.J. Herrero, *New Constraints on General Slepton Flavor Mixing*, *Phys. Rev.* **D 88** (2013) 015026 [arXiv:1304.2783] [INSPIRE].

[51] ATLAS collaboration, *Search for direct production of charginos, neutralinos and sleptons in final states with two leptons and missing transverse momentum in pp collisions at $\sqrt{s} = 8$ TeV with the ATLAS detector*, *JHEP* **05** (2014) 071 [arXiv:1403.5294] [INSPIRE].

JHEP10(2015)043

[52] CMS collaboration, *Searches for long-lived charged particles in pp collisions at $\sqrt{s} = 7$ and 8 TeV*, *JHEP* **07** (2013) 122 [arXiv:1305.0491] [INSPIRE].

[53] J.L. Feng, S.T. French, C.G. Lester, Y. Nir and Y. Shadmi, *The Shifted Peak: Resolving Nearly Degenerate Particles at the LHC*, *Phys. Rev.* **D 80** (2009) 114004 [arXiv:0906.4215] [INSPIRE].

[54] J.L. Feng et al., *Measuring Slepton Masses and Mixings at the LHC*, *JHEP* **01** (2010) 047 [arXiv:0910.1618] [INSPIRE].

[55] J. Eckel, M.J. Ramsey-Musolf, W. Shepherd and S. Su, *Impact of LSP Character on Slepton Reach at the LHC*, *JHEP* **11** (2014) 117 [arXiv:1408.2841] [INSPIRE].

[56] ATLAS collaboration, *Search for charginos nearly mass degenerate with the lightest neutralino based on a disappearing-track signature in pp collisions at $\sqrt{s} = 8$ TeV with the ATLAS detector*, *Phys. Rev.* **D 88** (2013) 112006 [arXiv:1310.3675] [INSPIRE].

[57] ATLAS collaboration, *Search for the direct production of charginos, neutralinos and staus in final states with at least two hadronically decaying taus and missing transverse momentum in pp collisions at $\sqrt{s} = 8$ TeV with the ATLAS detector*, *JHEP* **10** (2014) 96 [arXiv:1407.0350] [INSPIRE].

[58] R. Rattazzi and U. Sarid, *Large tan Beta in gauge mediated SUSY breaking models*, *Nucl. Phys.* **B 501** (1997) 297 [hep-ph/9612464] [INSPIRE].

[59] J. Hisano and S. Sugiyama, *Charge-breaking constraints on left-right mixing of stau's*, *Phys. Lett.* **B 696** (2011) 92 [*Erratum ibid.* **B 719** (2013) 472] [arXiv:1011.0260] [INSPIRE].

[60] R. Sato, K. Tobioka and N. Yokozaki, *Enhanced Diphoton Signal of the Higgs Boson and the Muon g-2 in Gauge Mediation Models*, *Phys. Lett.* **B 716** (2012) 441 [arXiv:1208.2630] [INSPIRE].

[61] T. Kitahara, *Vacuum Stability Constraints on the Enhancement of the $h \to \gamma\gamma$ rate in the MSSM*, *JHEP* **11** (2012) 021 [arXiv:1208.4792] [INSPIRE].

[62] L. Calibbi, J.M. Lindert, T. Ota and Y. Takanishi, *Cornering light Neutralino Dark Matter at the LHC*, *JHEP* **10** (2013) 132 [arXiv:1307.4119] [INSPIRE].

[63] M. Drees, H. Dreiner, D. Schmeier, J. Tattersall and J.S. Kim, *CheckMATE: Confronting your Favourite New Physics Model with LHC Data*, *Comput. Phys. Commun.* **187** (2014) 227 [arXiv:1312.2591] [INSPIRE].

[64] DELPHES 3 collaboration, J. de Favereau et al., *DELPHES 3, A modular framework for fast simulation of a generic collider experiment*, *JHEP* **02** (2014) 057 [arXiv:1307.6346] [INSPIRE].

[65] M. Cacciari, G.P. Salam and G. Soyez, *FastJet User Manual*, *Eur. Phys. J.* **C 72** (2012) 1896 [arXiv:1111.6097] [INSPIRE].

[66] M. Cacciari and G.P. Salam, *Dispelling the N^3 myth for the k_t jet-finder*, *Phys. Lett.* **B 641** (2006) 57 [hep-ph/0512210] [INSPIRE].

[67] M. Cacciari, G.P. Salam and G. Soyez, *The Anti-k(t) jet clustering algorithm*, *JHEP* **04** (2008) 063 [arXiv:0802.1189] [INSPIRE].

[68] A.L. Read, *Presentation of search results: The CL(s) technique*, *J. Phys.* **G 28** (2002) 2693 [INSPIRE].

JHEP10(2015)043

[69] J. Alwall et al., *The automated computation of tree-level and next-to-leading order differential cross sections and their matching to parton shower simulations*, *JHEP* **07** (2014) 079 [arXiv:1405.0301] [INSPIRE].

[70] T. Sjöstrand, S. Mrenna and P.Z. Skands, *PYTHIA 6.4 Physics and Manual*, *JHEP* **05** (2006) 026 [hep-ph/0603175] [INSPIRE].

[71] C.G. Lester and D.J. Summers, *Measuring masses of semiinvisibly decaying particles pair produced at hadron colliders*, *Phys. Lett.* **B 463** (1999) 99 [hep-ph/9906349] [INSPIRE].

[72] A. Barr, C. Lester and P. Stephens, *m(T2): The truth behind the glamour*, *J. Phys.* **G 29** (2003) 2343 [hep-ph/0304226] [INSPIRE].

[73] *Mt2 / Stransverse Mass / Oxbridge Kinetics Library*, http://www.hep.phy.cam.ac.uk/ lester/mt2/.

[74] H.-C. Cheng and Z. Han, *Minimal Kinematic Constraints and m(T2)*, *JHEP* **12** (2008) 063 [arXiv:0810.5178] [INSPIRE].

[75] N. Arkani-Hamed, H.-C. Cheng, J.L. Feng and L.J. Hall, *Probing lepton flavor violation at future colliders*, *Phys. Rev. Lett.* **77** (1996) 1937 [hep-ph/9603431] [INSPIRE].

[76] N. Arkani-Hamed, J.L. Feng, L.J. Hall and H.-C. Cheng, *CP violation from slepton oscillations at the LHC and NLC*, *Nucl. Phys.* **B 505** (1997) 3 [hep-ph/9704205] [INSPIRE].

[77] ATLAS collaboration, *Search for direct production of charginos and neutralinos in events with three leptons and missing transverse momentum in 21 fb^{-1} of pp collisions at $\sqrt{s} = 8$ TeV with the ATLAS detector*, ATLAS-CONF-2013-035 (2013).

[78] I. Galon and Y. Shadmi, *Kinematic Edges with Flavor Splitting and Mixing*, *Phys. Rev.* **D 85** (2012) 015010 [arXiv:1108.2220] [INSPIRE].

JHEP10(2015)043